Reduced Space Optimal Analysis for Historical Data Sets: 136 years of Atlantic Sea Surface Temperatures

Alexey Kaplan, Yochanan Kushnir, Mark A. Cane, and M. Benno Blumenthal

Lamont–Doherty Earth Observatory of Columbia University

Palisades, NY 10964

Accepted for publication in the *Journal of Geophysical Research – Oceans*, May 1997

Abstract.

A computationally efficient method for analyzing meteorological and oceanographic historical data sets has been developed. The method combines data-reduction and least squares optimal estimation. The data-reduction involves computing empirical orthogonal functions (EOFs) of the data based on their recent, high-quality portion and using a leading EOF subset as a basis for the analyzed solution and for fitting a first order linear model of time transitions. We then formulate optimal estimation problems in terms of the EOF projection of the analyzed field to obtain reduced space analogues of the optimal smoother, the Kalman filter, and optimal interpolation techniques. All reduced space algorithms are far cheaper computationally than their full grid prototypes, while their solutions are not necessarily inferior since the sparsity and error in available data often make estimation of small scale features meaningless. Where covariance patterns can be estimated from the available data, the analysis methods fill gaps, correct sampling errors, and produce spatially and temporally coherent analyzed data sets. As with classical least squares estimation, the reduced space versions also provide theoretical error estimates for analyzed values.

The methods are demonstrated on Atlantic monthly sea surface temperatures (SST) anomalies for 1856–1991 from the UK Meteorological Office historical sea surface temperature data set (version MOHSST5). Choice of a reduced space dimension of 30 is shown to be adequate. The analyses are tested by withholding a significant part of the data and prove to be robust and in agreement with their own error estimates; they are also consistent with a partially independent optimal interpolation (OI) analysis of Reynolds and Smith (1994) produced in the National Centers for Environmental Prediction (NCEP) (known as the NCEP OI analysis).

A simple statistical model is used to depict the month-to-month SST evolution in the optimal smoother algorithm. Results are somewhat superior to both the Kalman filter which relies less on the model, and the optimal interpolation which does not use it at all. The method generalizes a few recent works on using a reduced space for data set analyses. Difficulties of methods which simply fit EOF patterns to observed data are pointed out and the more complete analysis procedures developed here are suggested as a remedy.

1. Introduction

Systematic measurements of meteorological and oceanographic variables near the ocean's surface have more than a century and a half of history. Initially concentrated along well-defined ship tracks, these observations underwent rapid growth in recent decades and are lately supplemented by satellite observations to achieve unprecedented coverage. It is customary to average available data in regular longitude–latitude bins with quality control and other statistics (e.g. Comprehensive Ocean–Atmosphere Data Set (COADS) – Woodruff et al. 1987, or Global Ocean Surface Temperature Atlas (GOSTA) – Bottomley et al. 1990). However, the resulting data sets are characterized by large temporal non-uniformity in data availability and quality: recent decades are much richer in data than the beginning of the century, which in turn has much more data than the middle of the nineteenth century. In addition to this systematic non-uniformity, the data suffer from seasonal oscillations in availability and from abrupt changes in marine traffic that reflect important world events. Examples include the profound decrease in data coverage during the two world wars, leaps in data abundance in the Arabian Sea data after 1869 and on both sides of the Isthmus of Panama after 1914. For more comprehensive descriptions of the marine data record see Smith et al. (1994), Reynolds and Smith (1994), and Folland and Parker (1995).

The pressing importance of historical data sets for climate studies has motivated work on their analysis. Ideally, the analysis of an historical data set corrects observational error (which consists of instrumental and sampling errors) and fills gaps by values close to correct ones. The latter task is accomplished by carrying information from data-rich times and places to data-poor ones. Consequently, the analysis procedure should be able to move information around both in time and space.

Given a model (dynamical or statistical) to constrain the analysis, we can form a quadratic cost function $\mathbf{S}$ which will "punish" analyzed solutions in some properly weighted manner both for deviation from observed values and for discrepancies with the model equations. We can then minimize $\mathbf{S}$ unconditionally in a "variational analysis." Such a minimization uses the model as a "weak" constraint (Sasaki 1970). The "strong" constraint formulation (which requires the model be satisfied precisely) is inappropriate here, since the error in models for historical data

sets (especially for those used in this work) can be larger than the observational error.

In some variational analyses, the attitude towards weighting coefficients in cost functions is that "the weights can be thought of as empirically determined tuning parameters" (Legler et al. 1989, p. 711). Although there are objective ways to choose the weights, e.g. a method of generalized cross validation (GCV, Wahba et al. (1995), and references therein), we retreat to a more "classical" approach: if the model is linear (or linearized), then choosing weighting coefficients to be the inverse error covariance matrices will turn a minimizer of **S** into a classical least squares estimate (LSE). The attractive feature of LSE is its optimality; it has the smallest error variance among all linear unbiased estimates (Gauss – Markov theorem, see e.g. Mardia et al., 1979), and it is the best even in a more general class of estimates, if additional assumptions of normality are made. Of course, we do not know the error covariance matrices precisely, and we can estimate only their crudest features. Even GCV procedures, in their plausible applications, can help in optimal tuning of only few parameters; they cannot resolve all the details of covariance matrices.

A prognostic model, which acts both in space and time, is especially useful for analysis of a historical data set. Ideally, information can propagate both forward and backward in time, and in all spatial directions. Such an approach is known as an "optimal smoother" (OS) and there are different algorithms to implement it. We will use exclusively the Rauch–Tung–Striebel (RTS) algorithm, described in Rauch et al. (1965). Such algorithms, however, are too costly and inefficient for full grid representations of historical climate data sets with realistic dimensions. These problems can be solved by transforming the data from a full grid representation of spatial dimensions of a data set to a space of lesser dimension, namely to a space of the leading spatial empirical orthogonal functions (EOFs) of that field (Cane et al., 1996). Such an approach drastically decreases the computational cost, and allows the creation of a prognostic model for a data set, i.e. a multivariate first order autoregressive model (Markov model (MM)) for the time evolution of a vector of EOF amplitudes.

There are different ways to achieve the space dimension reduction. Fukumori and Malanotte-Rizzoli (1995) introduced the suboptimal KF where Kalman gains are calculated on a coarse subgrid of the model grid and then are interpolated on the entire grid; Fukumori

(1995) used the same approach for OS. Cohn and Todling (1996) compare three suboptimal KF schemes with reduced computational cost: one close to that of Fukumori and Malanotte-Rizzoli (1995), a reduced resolution filter; one somewhat similar to that of Cane et al. (1996), a partial eigendecomposition filter; and one which effectively reduces the rank of the model operator, a partial singular value decomposition filter. Thacker and Lewandowicz (1996) emphasize the role of principal components as "indices with maximum global skill." In the present work explicit use of a fixed low-dimensional linear subspace as a model space for analysis allows the interpretation of our statistical procedure, suboptimal in the space of full grid representations of the data, as an optimal LSE in the reduced space. This allows for a consistent derivation of the entire sequence of reduced space estimates: optimal interpolation (OI), KF, and OS.

Computational cost is not the only reason to reduce the dimension of the system space. Frequently there are not enough data to resolve small scales in estimating full grid error covariance (Dee 1995). As a result, the a priori covariance information on small scales in full grid data assimilation does more harm than good. Moreover, the assimilation for those scales represents the major computational expense of the entire procedure. The absence of small scale errors generously compensates the reduced space approach for both formal loss of optimality and actual loss in resolution. A case like that is documented in Cane et al. (1996), where the solution in the reduced KF is not inferior to the standard full grid KF solution.

The MM and its error covariance matrix can be constructed from the data by a linear best fit method. As far as the verisimilitude of such a statistical model is concerned, it is possible that a low order model acting in EOF space, where the major part of a signal lies, will capture the rudimentary dynamical features of the system (e.g. Blumenthal 1991, Xue et al. 1994). The OS can then use this dynamical information in order to constrain the fields in the data-poor periods. In the unfortunate case where the MM turns to be a complete failure, the corresponding terms in the cost function will still play a regularizing role by prohibiting excessively sharp time transitions in periods with poor data coverage. Our use of MM as a time-marching model in the reduced space OS procedure assumes that, in the absence of other information, the same large scale patterns which slowly evolve in the present, were similarly slowly evolving in the past.

Here we develop a computationally feasible way to produce a spatially and temporally

coherent analysis of a historical data set. We compute EOF patterns on the basis of available observations. Thus the method can run solely on the basis of a data set to be analyzed and does not require use of any additional information.

Our method generalizes the work of Cane et al. (1996) in the same sense in which OS generalizes KF. In a different sense, the method also generalizes the technique of Shriver and O'Brien (1995) and Smith et al. (1996); i.e. a least squares fit of EOFs to observations carried out separately at each time. This approach is also applied in Shen et al. (1994) to optimal averaging (OA). We will refer to this method as "projection." If there are no missing data, and the observational error is spatially uniform, this form of analysis is a simple orthogonal projection of the data on the reduced space. It will be shown in Section 2 that the projection method, as well as the reduced space analogue to a more sophisticated optimal interpolation (OI) technique (in the form described in Gandin, 1963) and reduced space KF, all can be reproduced by our method when certain parts of the cost function are dropped. In its most complete form this cost function produces a reduced space OS solution. For all these different kinds of analyzed fields our technique also supplies error estimates. This advantage of our approach is due to its probabilistic nature; it is absent in the projection method with its deterministic function fitting approach.

As a practical demonstration of the method, we analyze a sea surface temperature (SST) historical data set. This choice is motivated by the importance of SST history in monitoring past climate variability (Bottomley et al. 1990, Parker et al. 1994, Folland and Parker 1995, Smith et al. 1996). For this first practical application of the method we restrict our attention to the relatively data-rich Atlantic basin, but cover the entire time interval 1856–1991.

The plan of the paper is as follows. The next section presents the formalism of our method. Section 3 describes the details of its application to the analysis of 136 years of Atlantic SST. The results of the analysis are presented in section 4, along with robustness and internal consistency checks, as well as the results of cross-verification and comparison with the partially independent data of Reynolds and Smith (1994). Comparison with the projection method of Smith et al. (1996) is also presented there. Results are discussed in section 5, and conclusions are presented in section 6.

2. Methodology

2.1 Variational principle

Our goal is to estimate values of a physical variable $\mathcal{T}$ which changes with location and time. Let $\{\mathcal{T}_n\}$ represent a set of gridded fields of $\mathcal{T}$, which are rearranged as column vectors of dimension M, in order of ascending time $n = 1, \ldots, N$. Let $\mathcal{T}_n^o$ be a vector of available observations for components of $\mathcal{T}_n$ with random error ε_n^o:

$$\mathcal{T}_n^o = H_n \mathcal{T}_n + \varepsilon_n^o, \quad n = 1, \ldots, N. \tag{1}$$

Here H_n is the matrix which puts a complete field into the format of observations available for time n. If the observations are on the same grid as the analysis, H_n samples those points where data are available; otherwise H_n interpolates from the analysis grid to observational points. The observational error ε_n^o is expected to have zero mean and known spatial covariance R_n. This error is also assumed to be white in time and uncorrelated with the signal.

Suppose that in addition to observations we have a linear model A_n relating $\mathcal{T}_n$ at successive times:

$$\mathcal{T}_{n+1} = A_n \mathcal{T}_n + \varepsilon_n^{\mathrm{m}}, \quad n = 1, \ldots, N-1, \tag{2}$$

where the random single-step error $\varepsilon_n^{\mathrm{m}}$ is assumed to have zero mean, spatial covariance Q_n, and to be white in time and uncorrelated with the signal. Furthermore, we assume that ε^o and ε^{m} are uncorrelated for all times.

In the situation described above, the classical least squares estimate (LSE) of $\{\mathcal{T}_1, \mathcal{T}_2, \ldots, \mathcal{T}_N\}$ is the set of fields $\{\hat{\mathcal{T}}_1, \hat{\mathcal{T}}_2, \ldots, \hat{\mathcal{T}}_N\}$ for which a quadratic cost function

$$\begin{aligned} \mathbf{S}[\mathcal{T}_1, \mathcal{T}_2, \ldots, \mathcal{T}_N] = \textstyle\sum_{n=1}^{N} (H_n \mathcal{T}_n - \mathcal{T}_n^o)^T R_n^{-1} (H_n \mathcal{T}_n - \mathcal{T}_n^o) + \\ \textstyle\sum_{n=1}^{N-1} (\mathcal{T}_{n+1} - A_n \mathcal{T}_n)^T Q_n^{-1} (\mathcal{T}_{n+1} - A_n \mathcal{T}_n) \end{aligned} \tag{3}$$

reaches its minimum (cf. Appendix A).

This means that the minimum $\{\hat{\mathcal{T}}_1, \hat{\mathcal{T}}_2, \ldots, \hat{\mathcal{T}}_N\}$ is the best estimate, in a very natural sense, of $\mathcal{T}$ on the chosen space and time grids. This solution makes the best possible use of all available information: observations, model, and their error estimates (cf. Talagrand (1996)). It is an unbiased estimate of the physical field $\mathcal{T}$ with minimum (among all linear unbiased

estimates) variance of error (this follows from the Gauss–Markov theorem, e.g. Mardia et al. (1979), Rao (1973)). Such estimates are known as BLUEs (Best Linear Unbiased Estimates). If it is assumed that the error distribution is Gaussian, then from a Bayesian perspective the least squares solution can be interpreted as a maximum likelihood estimate, i.e. the *most probable* solution (Gelb 1974, pp. 103–104). If the errors *and the signal* are Gaussian random values, the solution turns out to be optimal among all, even non-linear estimates, and not only for minimum mean-square error criterion, but for a wide class of optimality criteria (Gelb, 1974 quotes Laning and Battin, 1956 to this effect, but it also follows from Theorem 2 of the famous work by Kalman, 1960).

Lorenc (1986) assumed a Gaussian error distribution in order to exploit the maximum likelihood features of estimates from various kinds of analysis. He emphasized the similarity among different methods of data analysis requiring the minimization of quadratic functions, e.g. variational methods, OI, KF, and OS (the last is only implicitly present in his paper). What is important here is that this similarity between different kinds of analysis exists even without any assumption of normality: all these methods, if their assumptions hold, give unbiased estimates, optimal in the class of linear unbiased estimates. The basic reason is that all of them construct LSEs out of given bits of information, as e.g. Sorenson (1970) illustrates by establishing a close connection between the original least squares method developed by Carl Friedrich Gauss in 1795 for his astronomical studies, and the Kalman filter theory.

2.2 Reduced space approach

Following Cane et al. (1996) we first make a transformation to the set of spatial EOFs (eigenvectors of the system's spatial covariance matrix). We then truncate that set to a much smaller subset which captures most of the signal. We write

$$\mathcal{T}_n = E\alpha_n + \varepsilon_n^r, \quad n = 1, \ldots, N,$$

where E is matrix whose columns are EOFs, α_n is a column vector containing the temporal amplitudes of the retained EOFs, and ε_n^r designates the error due to the space reduction (truncation). E is dimensioned $M \times L$ where M is the spatial dimension of $\mathcal{T}_n$ and $L \ll M$ is the number of EOFs retained.

In the present study, as in all data studies, the covariance matrix of observed field contains observational noise. An important reason for the popularity of EOFs is that the leading EOFs contain much of the variance of the signal and little of the noise, while the higher modes are largely noise (see Preisendorfer, 1988). This means that truncation of the high modes serves as a filter. For illustration consider white observational (plus sampling) noise, uniform in space, with variance δ^2, added to a signal which is independent of the noise. If the signal is presented on a grid of spatial dimension M and its spatial covariance matrix is C, the covariance matrix calculated from observations will be $C + \delta^2 I_M$. Let $\mathrm{Tr}[C] = S^2$, and transform to the reduced space of L leading EOFs which retains a ratio r of the total variance S^2. Since an identity matrix is invariant with respect to an orthogonal rotation, the noise variance in the reduced space will be $L\delta^2/M$. The signal-to-noise ratio in the reduced space will thus be $(r(S^2+\delta^2) - L\delta^2/M)/(L\delta^2/M)$, approximately rM/L times larger than the original ratio of S^2/δ^2. In the present work, characteristic parameters are $r = 0.78$, $L = 30$, and $M = 275$. Hence the "effectiveness" of the space reduction $rM/L = 7.2$.

It is well known (North et al. (1984), Cheng et al. (1995)) that the patterns of individual EOFs are unstable to perturbations of C. Fortunately for the present application, a linear subspace spanned by the first few EOFs is a much more robust object (despite the fact that individual EOFs themselves can be strongly distorted by "mixing up" in "effectively degenerate multiplets").

Time connection in the analysis is provided by a version of (2) in the reduced space:

$$\alpha_{n+1} = \mathcal{A}_n \alpha_n + \check{\varepsilon}^{\mathrm{m}}_n, \quad \left\langle \check{\varepsilon}^{\mathrm{m}} \check{\varepsilon}^{\mathrm{m\,T}} \right\rangle = \mathcal{Q}_n$$

For full grid representation we have

$$A_n = E\mathcal{A}_n E^T, \quad Q_n = E\mathcal{Q}_n E^T \tag{4}$$

Using (4) and the orthogonality of retained and discarded modes, (1,2) may be transformed to the reduced space:

$$\mathcal{T}^o_n = H_n E \alpha_n + (H_n \varepsilon^r_n + \varepsilon^o_n) \stackrel{\mathrm{def}}{=} \mathcal{H}_n \alpha_n + \check{\varepsilon}^o_n, \quad n = 1, \ldots, N, \tag{5}$$

$$\alpha_{n+1} = \mathcal{A}_n \alpha_n + E^T \varepsilon_n^{\mathrm{m}} \stackrel{\mathrm{def}}{=} \mathcal{A}_n \alpha_n + \check{\varepsilon}_n^{\mathrm{m}}, \quad n = 1, \ldots, N-1. \tag{6}$$

With the additional assumption that the truncation error ε_n^r is uncorrelated with other types of error and has zero mean, and after neglecting the possible non-whiteness of the sequence $(H_n \varepsilon_n^r + \varepsilon_n^o)$ (due to the time correlation of ε_n^r), the reduced state space scheme (5,6) is similar to the full grid scheme (1,2) with a new "observational" error $\check{\varepsilon}_n^o$ and a new model error $\check{\varepsilon}^{\mathrm{m}}$. Note that to use this similarity, the truncation error must be uncorrelated with the retained modes, so the solution obtained is a projection of the full grid optimal solution on a reduced space. Otherwise, the new "observational" error is correlated with the "signal," and we find ourselves outside of the classical scheme of the least squares approach. If the EOFs which span the reduced space are eigenvectors of the true signal covariance matrix, the requirement of independency is automatically satisfied. In practice we make the assumption that the correlation is small.

Now

$$\mathcal{Q}_n = \langle \check{\varepsilon}_n^{\mathrm{m}} \check{\varepsilon}_n^{\mathrm{m}\,T} \rangle = E^T \langle \varepsilon_n^{\mathrm{m}} \varepsilon_n^{\mathrm{m}\,T} \rangle E = E^T Q_n E$$

(viz (4)), and the reduced space analogue of the observational error covariance matrix is

$$\mathcal{R}_n = \langle \check{\varepsilon}_n^o \check{\varepsilon}_n^{o\,T} \rangle = \langle (H_n \varepsilon_n^r + \varepsilon_n^o)(H_n \varepsilon_n^r + \varepsilon_n^o)^T \rangle =$$
$$\langle \varepsilon_n^o \varepsilon_n^{o\,T} \rangle + H_n \langle \varepsilon_n^r \varepsilon_n^{r\,T} \rangle H_n^T \stackrel{\mathrm{def}}{=} R_n + H_n C^r H_n^T \stackrel{\mathrm{def}}{=} R_n + R_n'. \tag{7}$$

By analogy with (3), a cost function for a reduced space estimation problem (5,6) is

$$\mathcal{S}[\alpha_1, \alpha_2, \ldots, \alpha_N] = \textstyle\sum_{n=1}^{N} (\mathcal{H}_n \alpha_n - \mathcal{T}_n^o)^T \mathcal{R}_n^{-1} (\mathcal{H}_n \alpha_n - \mathcal{T}_n^o) +$$
$$\textstyle\sum_{n=1}^{N-1} (\alpha_{n+1} - \mathcal{A}_n \alpha_n)^T \mathcal{Q}_n^{-1} (\alpha_{n+1} - \mathcal{A}_n \alpha_n). \tag{8}$$

Below we consider minimization of $\mathcal{S}$ in its full (OS) or somewhat truncated versions (KF,OI, and projection).

(a). Kalman Filter. Hereafter superscripts a and f will correspond to the analysis and forecast stages of the KF, respectively. The variables (α_n^f, $\mathcal{P}_n^f$, α_n^a, $\mathcal{P}_n^a$) are computed according to the standard KF formalism (e.g. Gelb 1979; Ghil et al., 1981):

$$\alpha_n^a = \alpha_n^f + \mathcal{K}_n \left(\mathcal{T}_n^o - \mathcal{H}_n \alpha_n^f \right),$$

$$
\begin{aligned}
&\alpha_n^f = \mathcal{A}_n \alpha_{n-1}^a, \\
&\mathcal{K}_n = \left(\mathcal{H}_n^T \mathcal{R}_n^{-1} \mathcal{H}_n + \mathcal{P}_n^{f\,-1}\right)^{-1} \mathcal{H}_n^T \mathcal{R}_n^{-1} \\
&\mathcal{P}_n^a = (I_L - \mathcal{K}_n \mathcal{H}_n)\mathcal{P}_n^f \\
&\mathcal{P}_n^f = \mathcal{A}_{n-1} \mathcal{P}_{n-1}^a \mathcal{A}_{n-1}^T + \mathcal{Q}_{n-1}, \qquad n = 2, 3, \ldots, N
\end{aligned}
\tag{9}
$$

with initial conditions

$$
\alpha_1^f = \alpha_1^a = \mathcal{P}_1^a \mathcal{H}_1^T \mathcal{R}_1^{-1} \mathcal{T}_1^o, \qquad \mathcal{P}_1^a = \mathcal{P}_1^f = \left(\mathcal{H}_1^T \mathcal{R}_1^{-1} \mathcal{H}_1\right)^{-1}, \tag{10}
$$

which correspond to minimization of the first term only in the first summation in (8). The connection between the general expression (8) and KF is that the analysis α_n^a of KF can be derived in a form analogous to (8) by performing the minimization of $\mathcal{S}[\alpha_1, \alpha_2, \ldots, \alpha_n]$ for $2 \le n \le N$ and taking only the n-th field of the result.

(b). Optimal smoother: If the RTS algorithm (Rauch et al. 1965) is applied to the reduced space version $\mathcal{S}$ instead of to $\mathbf{S}$ the computation is far cheaper: the M-dimensional full grid space vector $\mathcal{T}_n$ is replaced by the L-dimensional ($L \ll M$) reduced space vectors α_n. (A remaining potential difficulty, inverting the observational error covariance matrix $\mathcal{R}_n$ at every timestep, is discussed in section 3.3). Minimization of $\mathcal{S}$ by the RTS algorithm gives a reduced space version of OS. The initial (ascending in time) sweep of the RTS algorithm is a run of the KF (9), while the second, reverse, time sweep modifies the KF estimates on the basis of future observational data

$$
\begin{aligned}
&\alpha_n^s = \alpha_n^a + G_n \left(\alpha_{n+1}^s - \mathcal{A}_n \alpha_n^a\right), \\
&G_n = \mathcal{P}_n^a \mathcal{A}_n^T (\mathcal{P}_{n+1}^f)^{-1}, \\
&\mathcal{P}_n^s = \mathcal{P}_n^a + G_n \left(\mathcal{P}_{n+1}^s - \mathcal{P}_{n+1}^f\right) G_n^T, \qquad n = N-1, \ldots, 2, 1
\end{aligned}
$$

with initial conditions

$$
\alpha_N^s = \alpha_N^a, \qquad \mathcal{P}_N^s = \mathcal{P}_N^a.
$$

(c). Optimal interpolation. Let $\mathcal{A}_n = 0$, eliminating the connection between sequential times. Correspondingly, replace $\mathcal{Q}_n$ in (8) by the field covariance matrix $\mathcal{C}_{n+1}$ at time $n+1$. As a result, the analyzed field for each time is unrelated to any other time. It minimizes (8) in the

form

$$\mathcal{S}_n^{\mathrm{OI}}[\alpha_n] = (\mathcal{H}_n\alpha_n - \mathcal{T}_n^o)^T\mathcal{R}_n^{-1}(\mathcal{H}_n\alpha_n - \mathcal{T}_n^o) + \alpha_n^T\mathcal{C}_n^{-1}\alpha_n, \qquad n > 1, \tag{11}$$

which is the cost function of Gandin's (1963) OI procedure[1]. The estimate α_n^{OI} and its error $\mathcal{P}_n^{\mathrm{OI}}$ from this procedure are

$$\alpha_n^{\mathrm{OI}} = \mathcal{P}_n^{\mathrm{OI}}\mathcal{H}_n^T\mathcal{R}_n^{-1}\mathcal{T}_n^o, \quad \mathcal{P}_n^{\mathrm{OI}} = \left(\mathcal{H}_n^T\mathcal{R}_n^{-1}\mathcal{H}_n + \mathcal{C}_n^{-1}\right)^{-1}. \tag{12}$$

Interpretation of the OI solution as a Gauss–Markov estimation is obvious: the OI estimate is a LSE when α_n is "observed" to be zero with error covariance $\mathcal{C}_n$. When α_n has zero mean ($\mathcal{T}$ is anomaly), this interpretation is perfectly legitimate.

There is another interesting interpretation for the second term in (11). Since $\mathcal{C}_n = E^T C_n E = \Lambda_n$ is a diagonal matrix of eigenvalues in the reduced space,

$$\alpha^T\mathcal{C}^{-1}\alpha = \alpha^T\Lambda^{-1}\alpha = \sum_{i=1}^{L}\frac{\alpha_i^2}{\lambda_i}.$$

Thus the second term of the cost function is a constraint on the EOF-spectrum of the solution: the higher the mode, the smaller is λ_i and the more severe is the "punishment" for deviation of its amplitude from zero. The OI solution is thus discouraged from giving too much energy to the features which "historically" had little energy.

(d). Projection. If the second term is dropped in (8) (or 11),

$$\alpha_n^p = \mathcal{P}_n^p\mathcal{H}_n^T\mathcal{R}_n^{-1}\mathcal{T}_n^o, \qquad \mathcal{P}_n^p = (\mathcal{H}_n^T\mathcal{R}_n^{-1}\mathcal{H}_n)^{-1} \tag{13}$$

This approach is very close to a method of analysis employed by Shriver and O'Brien (1995) and Smith et al. (1996) (though with some differences; see Sec. 5.).

(e). Verification of error estimates. For all estimates $\hat{\alpha}$ presented in this section a full grid representation $\hat{\mathcal{T}}$ of the solution can be recovered by formulae

$$\hat{\mathcal{T}} = E\hat{\alpha}, \qquad P = E\mathcal{P}E^T \tag{14}$$

---

[1]We use the term OI throughout the paper in this original sense of Gandin; this sense is different from the modern usage, in which OI basically denotes KF with disabled (or simplified) covariance evolution procedure

(dropping the time index n). The error covariance P in (14) corresponds to the error in patterns spanning the reduced space only. To obtain the error in comparison to the true field $\mathcal{T}$ in a full grid space, we have to account for the error of reduction:

$$\hat{\mathcal{T}} - \mathcal{T} = E(\hat{\alpha} - \alpha) + (E\alpha - \mathcal{T}) = \varepsilon + \varepsilon^r.$$

Since the error of reduction ε^r enters the analysis, it is correlated with the analysis error ε. Hence the full grid error covariance in the reduced space estimate $\hat{\mathcal{T}}$ is

$$\Pi = \langle(\hat{\mathcal{T}} - \mathcal{T})(\hat{\mathcal{T}} - \mathcal{T})^T\rangle = P + \langle\varepsilon\varepsilon^{r\,T}\rangle + \langle\varepsilon^r\varepsilon^T\rangle + C^r. \tag{15}$$

The traces of the cross terms here are equal to zero, since ε and ε^r belong to two mutually orthogonal spaces of retained and discarded patterns. Consequently those terms do not change the total variance of the error in the entire area of analysis, but rather redistribute it. For an error estimate which is easy to compute, and which holds for any single point in the domain or for subdomain averages, we can use an inequality[2]

$$\Pi \leq 2(P + C^r),$$

which immediately follows from the fact that

$$0 \leq \langle(\varepsilon - \varepsilon^r)(\varepsilon - \varepsilon^r)^T)\rangle = P + C^r - (\langle\varepsilon\varepsilon^{r\,T}\rangle + \langle\varepsilon^r\varepsilon^T\rangle).$$

The consistency of the analysis can be verified by comparing analyzed fields with the data and checking if the analysis-data discrepancy agrees with the theoretical estimates of the error, produced by the analysis procedure. To get the theoretical estimate for the covariance of the discrepancy between data and analysis, we have to distinguish between the cases when data *are* or *are not* used in producing the analysis estimate.

- *The data* were not *used in producing the analysis estimate.* In this case observational and analysis' errors are independent,

$$\langle(H\hat{\mathcal{T}} - \mathcal{T}^o)(H\hat{\mathcal{T}} - \mathcal{T}^o)^T\rangle = H\Pi H^T + R. \tag{16}$$

[2]Symmetric matrices (quadratic forms) A and B are said to be in relation $A \leq B$ if $x^T Ax \leq x^T Bx$ for all vectors x (or, equivalently, if $(B - A)$ is non-negative definite)

- *The data* were *used in producing the analysis estimate.* In this case

$$\langle (H\hat{\mathcal{T}} - \mathcal{T}^o)(H\hat{\mathcal{T}} - \mathcal{T}^o)^T \rangle = \mathcal{R} - HPH^T, \tag{17}$$

which turns to be a generic formula for all LSE methods (cf. Miller (1990, p. 11,466) and Cane et al. (1996) for KF case).

(f). Error estimates for subdomain averages. Computing subdomain average of an optimal solution gives an estimate known as that of "optimal averaging" (OA) (see e.g. Smith et al. 1994), and, naturally, produces a theoretical error estimate for it which takes into account spatial error correlation. Suppose χ is an index column vector denoting the corresponding subdomain (i.e. $\chi_i = 1$ if a point with spatial index i is included into the subdomain, and $\chi_i = 0$ otherwise). The spatial average for the field estimate $\overline{\mathcal{T}} = c\chi^T W\hat{\mathcal{T}}$, where W is a diagonal matrix of gridbox area weights, and $c = (\chi^T W\chi)^{-1}$ is a normalizing factor making the sum of the weights equal unity. The error in $\overline{\mathcal{T}}$ is equal to $c\chi^T W(\varepsilon + \varepsilon^r)$, and thus the error variance is

$$\sigma^2 = c^2\chi^T W\Pi W\chi \le 2c^2\chi^T W(P + C^r)^T W\chi = 2(x^T\mathcal{P}x + x^{r\,T}\Lambda^r x^r), \tag{18}$$

where $x = cE^T W^{1/2}\chi$ and $x^r = cE^{r\,T}W^{1/2}\chi$ are vectors whose components are results of averaging the retained (E) and discarded (E^r) EOF patterns, respectively (Λ^r is a diagonal matrix of eigenvalues (energies) corresponding E^r).

3. Practical application

3.1 Data set for analysis

We demonstrate the method of reduced space optimal analysis by applying it to a historical sea surface temperature (SST) data set for the relatively data-rich Atlantic basin (102.5°W–22.5°E and 42.5°S–82.5°N). Our method assumes that all errors are random. However, trends and biases appear in many historical data sets (for SST see Barnett 1984, Folland et al. 1984, Jones et al. 1991). Presence of a time-varying bias in an observational data set will result in the biased analysis: the portion of the bias changing slowly in time and displaying large spatial scales most likely will project well on the leading EOF patterns, and thus cannot be distinguished from physical signals by the analysis method presented here. Therefore we

use data extracted from the MOHSST5 product of the UK Meteorological office Global Ocean Surface Temperature Atlas (GOSTA) (Bottomley et al. 1990, Parker et al. 1994) which incorporates provisional corrections for time-varying biases as described in Folland and Parker (1995). Monthly SST anomalies from 1856 to 1991 are departures from 1951–1980 GOSTA climatological means. They are presented on a $5^o \times 5^o$ grid as averages of the observations available for each gridbox, and are attributed to the geometric centers of the gridboxes. That the actual observations are irregularly sampled inside the box is taken into account through a term in the observational error estimate corresponding to the natural variability of SST on a 5^o scale, as described in section 3.3. This estimate requires knowledge of the actual number of observations used for each gridbox estimate and also their standard deviations. The latter, which were not available from the UK Meteorological Office, were taken from data available in the COADS $2^o \times 2^o$ summaries (Woodruff et al. 1987).

Use of anomalies rather than full SST fields has several advantages. Taking away the seasonal cycle makes the EOF representation more effective, and makes the construction of a Markov model somewhat easier. In addition, a number of the steps in our procedure (filtering covariance matrix by Shapiro (1971) filter, space reduction, OI, use of variance–losing MM) have the downside of cutting some portion of the variance. In working with anomalies with zero means, we obtain unbiased results even when variance is lost.

Note that even on the coarse grid of 5 degrees, in the relatively well-sampled Atlantic basin, the inhomogeneity of data coverage over the entire period of 1856–1991 is striking (see Figure 11, Bottomley et al., 1990), which makes their analysis a demanding test for our methods.

3.2 Covariance matrix and EOFs

We used the relatively data rich period of 1951–1991 for the EOF calculation. Samples of all months were pooled to estimate the covariance of raw GOSTA data. We restrict the analysis to the $M = 275$ (out of 326) ocean gridpoints in the Atlantic which have at least 50% of the monthly data points available for the period of 1951–1991. We do not require that all gridboxes display a common period of data availability. Rather we calculate each element in the covariance matrix based on the common period of the two respective gridboxes, meaning that the sampling

errors of the data covariance matrix estimate $C_{\rm raw}$ vary from element to element due to the varying numbers of time points. For all elements of $C_{\rm raw}$, we have data available almost 45% of the time.

Our goal here is to estimate the true signal covariance C which is different from the data covariance $C_{\rm raw}$ because the latter contains observational error:

$$C_{\rm raw} = C + R$$

and, to make matter worse, is affected by data voids. Because of the latter and because our estimate of R is not faultless, we do not risk to estimate C by subtraction. Instead we apply the 4th order Shapiro filter (Shapiro 1971) in both the longitudinal and latitudinal directions to reduce random errors. An innovation here is that the filter was applied to data autocovariance patterns (the rows and columns of the sample covariance matrix) rather than to the patterns of observed data. Each row and column has an entry at each grid point, and the filter is applied to each as if to a data field (i.e., the covariances are smoothed in the geographical coordinates). If there were no gaps in the data, the result would be identical to the application of the filter in the data space. That is, the covariance of the filtered data is the same as the filtered covariance. To see this, let $\mathcal{L}$ be the linear filter and X the data vector, so that $\mathcal{L}X$ is the filtered data. Then

$$\langle(\mathcal{L}X)(\mathcal{L}X)^T\rangle = \mathcal{L}\langle XX^T\rangle\mathcal{L}^T = \mathcal{L}C_{\rm raw}\mathcal{L}^T;$$

the right-hand side is the operation we perform. Note that there is no straightforward way to filter the data directly when there are gaps.

While application of the Shapiro filter to the covariance matrix produces $C_{\rm f} = \mathcal{L}C_{\rm raw}\mathcal{L}^T$ with a reasonably "clean" correlation structure (one with the small scales strongly depleted), it also reduces the variance. We can obtain an estimate of the true variance by subtracting the estimate of observational error variance (constructed as in section 3.3 and averaged over the period 1951–1991) from data variance:

$$\mathrm{diag}[C] \approx \mathrm{diag}[C_{\rm raw} - R].$$

At locations where the variance after filtering $V_{\rm f} = \mathrm{diag}[C_{\rm f}]$ is smaller than this estimate, we

increase it to the estimated level. Thus:

$$\hat{V} = \max\{V_{\rm f}, \mathrm{diag}[C_{\rm raw} - R]\}$$

which corresponds to increasing the diagonal elements of $C_{\rm f}$ by the factors $F = \hat{V}/V_{\rm f}$. Whenever a diagonal element in the covariance matrix is increased, we also multiply elements in the corresponding row and column by the square root of the rate of increase, so that the resulting matrix $\hat{C}$ has $\hat{V}$ on diagonal, but defines exactly the same correlation patterns as those obtained after the Shapiro filtering. More formally,

$$\hat{C} = D^{\frac{1}{2}} C_{\rm f} D^{\frac{1}{2}},$$

where D is a diagonal matrix with the elements of the vector F on its diagonal.

The EOFs were calculated as eigenvectors of $\hat{C}$ with elements weighted by the appropriate gridbox areas. As usual, the leading EOFs are expected to represent reliable spatial patterns of the observed anomalies. The filtered data covariance matrix is not guaranteed to be positive–definite because of the gaps in the data. However, only the last 5 out of the 275 eigenvalues were negative (totaling $2 \cdot 10^{-4}$ of the trace) indicating that the covariance matrix was well estimated.

The sequence of eigenvalues λ'_m of $\hat{C}$ obtained directly from the EOF analysis decreases too steeply due to the depletion of small scales by the Shapiro filter. An incorrectly steep spectrum of eigenvalues can make the analysis too "optimistic" about the ratio of signal variance it apparently can constrain, yielding theoretical error estimates that are too small. This showed up as a failure of consistency tests (such as those described in Section 4.2*(a)*). To redistribute energy between EOFs (while preserving the total variance) by transferring it from large to small scales, we write

$$\lambda_m = (1-\beta)\lambda'_m + \frac{\beta}{M}\sum_{k=1}^{M} \lambda'_k, \qquad m = 1, \ldots, M \tag{19}$$

This redistribution depends on a single parameter β characterizing its "intensity," and is the smoothest change in the spectrum that preserves the variance. In this paper we use $\beta = 0.1$. The theoretical basis for the choice of a value for β is given in Appendix B.

Values of λ_m from (19) are used hereafter as the estimates of "true signal" eigenvalues.

Based on these estimates the first 5, 10, 20, 30, 50, and 75 EOFs explain 41%, 55%, 70%, 78%, 85%, and 90% of the variance respectively.

3.3 Constructing a priori data error estimates

The data error estimate $\mathcal{R}$ consists of two parts, observational error and truncation error; cf. (7). Errors in area averaged observational data are due to both instrumental errors and sampling errors: the former characterizes the accuracy of each individual measurement, and the latter accounts for the fact that observations are not direct measurements of a time and space averaged value over the gridbox. We assume independence of errors for measurements taken in different boxes. If there is in fact significant correlation between such errors (arising, for example, from systematic rather than random irregularity of sampling patterns inside boxes, or through strongly biased instruments on some individual "bad" ships), it will increase the "effective" observational error by lowering the actual number of degrees of freedom in the observed system (cf. Blumenthal and Cane (1989), their Appendix B), and will make the solution less optimal. However, at the present time there is no information which would allow to formulate a more elaborated model for observational error than a simple assumption of their mutual independency. It should be pointed out that reduced space analysis is much less sensitive to the detailed specification of the observational error covariance than traditional full grid schemes are (cf. formula (20)).

If deviations from the mean value within the box and month are random and independent, the sampling error variance can be estimated as σ^2/n_{obs}, where σ^2 is the observed field monthly intrabox variability, and n_{obs} is the number of intrabox measurements for the month (Legler (1991), Trenberth et al. (1992)). We obtained the number of observations from the UK Meteorological office on a $1^o \times 1^o$ box resolution, finer than that of SST estimates. If the actual number of observations per $1^o \times 1^o$ box for a given month was larger than 60, we used 60 in our calculation, assuming that more than 2 observations per day for such boxes do not bring independent information.

Since the intrabox variability σ^2 is not part of the GOSTA data set, we estimated it from COADS (Woodruff et al. 1987), which is presented on $2^o \times 2^o$ boxes. We used 1980–1992

COADS intrabox σ's and $n_{\rm obs}$'s to estimate intrabox variability for $4^o\times4^o$ and $6^o\times6^o$ boxes. The patterns of the two are similar, with the larger box being no more than about 50% higher. The variability for $5^o\times5^o$ boxes is estimated as an average of those two patterns (Figure 1). The most prominent feature is the high variability in the Gulf Stream separation region and south of Newfoundland. By construction, our estimate of intrabox variability accounts also for instrumental error in the observed data. Observational error rms for 41-year-periods at the beginning and at the end of analysis interval are shown in Figure 2 as well as the variance in time of the domain average. The magnitudes of the error for modern data are fairly consistent with those inferred in Trenberth et al. (1992).

Because of the EOF truncation, we have to account for $R'_n = H_n C^r H_n^T$ (cf. (7)), the part of the covariance that falls into the discarded modes:

$$\mathcal{R}_n = R_n + H_n C^r H_n^T = R_n + H_n E^r \Lambda^r E^{r\,T} H_n^T, \tag{20}$$

where R is the diagonal matrix of observational error (with elements $\sigma^2/n_{\rm obs}$). Since $\mathcal{R}_n$ is a non-diagonal square matrix of the order of number of observations, its inversion each time step can be expensive. To reduce the cost, we subdivide the truncation error term in (20) into parts corresponding to patterns of intermediate scale (with numbers between $L+1$ and $4L$ which represent spatial scales down to half of the smallest scale we retain in the reduced space solution) and those of small scale (with numbers larger than $4L$). The latter covariance can be well approximated by its diagonal:

$$H_n E^r \Lambda^r E^{r\,T} H_n^T = H_n E^r_{<4L} \Lambda^r_{<4L} E^{r\,T}_{<4L} H_n^T + H_n E^r_{>4L} \Lambda^r_{>4L} E^{r\,T}_{>4L} H_n^T \approx$$

$$\approx H_n E^r_{<4L} \Lambda^r_{<4L} E^{r\,T}_{<4L} H_n^T + \mathrm{diag}\left[H_n E^r_{>4L} \Lambda^r_{>4L} E^{r\,T}_{>4L} H_n^T\right].$$

As a result $\mathcal{R}$ is presented as a sum of a diagonal matrix with a product of two low-rank (of rank $3L$) matrices. This makes $\mathcal{R}$ easily invertible (in a $3L$-dimensional space) according to Sherman–Morrison–Woodbury formula (Householder, 1975).

The estimated truncation error rms for 30 modes is about 0.2–0.25^{o}C in the most of the domain, increasing to 0.3–0.4^{o}C towards its southern and northern boundaries. An independent verification of our observational error estimate can be derived from a comparison between

the GOSTA data and the NCEP OI analysis (Reynolds and Smith, 1994) assuming that the OI error is negligible compared to that of GOSTA. When rms differences between these two products were computed for the interval 1982–1991, the resulting pattern was similar to that of the estimated observational error, but with larger values. This discrepancy can be explained by noting that the NCEP OI analysis effectively reduces the analysis space by smoothing.

3.4 Construction of the Markov model

We construct the MM from time series of EOF expansion amplitudes obtained from the OI analysis. $\mathcal{A}_n$ is thus a Markov Model (MM) constructed from the available data. The actual dependence of $\mathcal{A}_n$ on n can be made seasonal or monthly (see Blumenthal 1991, Xue et al. 1994), or dropped altogether. Ideally we would like to have a model that fully captures the time transitions of a few tens of EOFs, but there are not enough data to estimate reliably all elements of such a model. This effectively restricts the size of the matrix $\mathcal{A}_n$, and also makes it reasonable to somehow predetermine its structure: to make it diagonal, banded, block-diagonal, etc. In each case, given the sequence $\{\alpha_n\}$, matrices $\mathcal{A}_n$ and $\mathcal{Q}_n$ with predetermined structure and type of time-dependence can be found by a linear best fit.

The MM was constructed on the amplitudes from OI solution in a space of dimension 50 for the period 1951–1991 (492 monthly samples). To determine the maximum number of EOFs which can be included into the meaningful first order MM, we compare the singular values of the lag-one covariance matrix for the actual sequence of OI amplitude vectors, with those obtained for 500 randomly reshuffled sets of the same vectors (Figure 3*(a)*). Singular values for the actual sequence are always larger than those for 95% of reshufflings, with the minimum ratio reached at the first time around the 30th mode (Figure 3*(b)*). The structure of the lag-one correlation matrix manifests strong diagonal dominance, and thus suggests a diagonal structure for the MM. The coefficients of the diagonal MM, when compared with reshuffled samples prove to be even more meaningful than the singular values of the lag-one covariance matrix, with a plateau reached around the 30th mode. We therefore chose L =30 to be the dimension of the MM.

To check if the available data resolve the seasonal dependence of the MM, we ran similar statistical tests for a seasonally dependent MM and found them to be much less significant than

those with no seasonal dependence. If the MM is taken to be dependent on the month of the year, its coefficients for different months oscillate irregularly around those for the MM with no time dependence. Furthermore, the error decrease by introducing seasonal dependence is negligible. Thus, we waive the seasonal dependence of the MM, and the model $\mathcal{A}$ we finally use in the analysis is simply a first-order autoregressive model for individual components of α_n^{OI}, i.e $\mathcal{A}$ is a fixed diagonal matrix with lag-one autocorrelations for components α_n^{OI} on its diagonal.

In addition we checked to see if the diagonal MM can be successfully corrected by some non-diagonal terms predicting the error of the diagonal MM. However, the singular values of the covariance matrix between the error of the diagonal MM and the OI amplitudes on the previous time were not distinguishable from those obtained for reshuffled sequences at the 95% level. We conclude that the diagonal MM which we chose for the analysis cannot be improved with the available data .

The chosen MM may be characterized as a model of "decaying persistence" in the EOF space: all it does to predict the SST field for the next month is to repeat the patterns of the present month with scaled down amplitudes. It leaves in place 90% of the amplitude for the first EOF, but only about 40% of the amplitude for the modes with numbers around 30. On average, predictions one month ahead reproduce about 60% of the signal variance.

The error estimate for MM is determined by

$$\mathcal{Q} = \Lambda - \mathcal{A}\Lambda\mathcal{A} = \Lambda(I - \mathcal{A}^2);$$

the last transformation assumes the diagonality of the MM.

Since L =30 EOFs gave the optimal MM, we compute the analyses with the reduced space of this dimension. However, it is possible to increase the dimension by letting the same MM predict as zeros the amplitudes of higher modes (in that case high order modes are treated as stationary).

4. Results

4.1 Data verification

To verify and tune the settings of our analysis procedures, we compared its results for 1982–1991 with the high-quality NCEP OI analysis (Reynolds and Smith, 1994), which makes use of buoy and satellite observations in addition to ship data. First, we use it to check the adequacy of our choice of the reduced space dimension $L = 30$. The OS analysis experiments were run for 1982–1991 with reduced spaces truncated to 5, 10, 20, 30, 50, and 75 EOFs. For each experiment the rms difference between the solution and the NCEP OI analysis is shown in Figure 4 (the NCEP OI data were first interpolated onto $5^o \times 5^o$ grid, and their reference climatology were adjusted to comply with the GOSTA climatology). As a number of EOFs increases the rms difference with the NCEP OI improves almost everywhere until $L = 30$. From $L = 30$ to $L = 50$ areas of improvement are about equaled by areas of degraded comparison; for $L = 75$ performance is worsened almost everywhere. Comparison of changes in rms with the patterns of observational error in Figure 2 shows that areas where the rms differences increase as L increases roughly correspond to areas with low-quality data. In going from $L = 50$ to $L = 75$ the analysis improves only in areas of high-quality data. Apparently, for $L > 30$ the analysis overfits observed data. For high-quality data, whose signal is more likely to stay in the NCEP OI solution, the present analysis is closer to the NCEP OI values, but overfitting low-quality data results in higher error and values farther from the NCEP OI solution. Incidentally, the variance corresponding to the first 30 EOFs is (roughly) complementary to the estimated observational error level (which was about 25% of the data variance for the sample of 1951-1991 for which EOFs were calculated).

Comparison of the OS analysis with 30 EOFs against the NCEP OI solution shows that except for the very northern part of the basin where ship-based sampling is generally poor and signal variance is high, the distribution of SST variance in the two analyses is very close (Figure 5). This is reassuring, since the reduced space OS solution might be expected to lose some part of the signal variance. The OS solution is slightly closer to the GOSTA data than the NCEP OI solution is, but the two analyses are much closer to each other than either of them is to the

GOSTA. Figure 6 demonstrates this by comparing the OS, GOSTA observations, and NCEP OI analysis in terms of their time dependent spatial rms difference and correlation. Note the drop in similarity between the NCEP OI and OS solutions at the end of 1991. This drop results from the increased difference between the GOSTA data and the NCEP OI during this year. The satellite and in situ data were clearly carrying different signals for the last four months of 1991, perhaps because satellite data was biased by both the Pinatubo eruption and a satellite calibration problem (cf. Reynolds and Smith, 1994).

4.2 Robustness and consistency of the analyses

Before analyzing the entire 136-year-long record, we carried out two experiments in order to check the robustness of the method and the consistency of its results with the error estimates which it produces.

(a). Experiment with withdrawn areas. To check how much the results of OS gap filling can be trusted, data over a large (30^o longitude$\times 20^o$ latitude) area was withdrawn from the analysis in three different regions: the North Atlantic, Tropical Atlantic, and South Atlantic. A typical result of these experiments is shown in Figure 7. The OS analysis proves to be very robust: the SST anomalies in the withdrawn areas are structurally close to the OS analysis with all data used. It should be noted that the EOFs and the MM were calculated from data for 1951–1991, a period that does not include the data shown in Figure 7.

To check the consistency of error estimates, we compare the rms differences between the standard OS analysis for the period of 1946–1991 and its versions with areas of withheld data, against the average of theoretical error estimates from the runs with withheld data (Figure 8). Note that the differences between OS runs are concentrated in the areas where data were withdrawn, while error estimates also recognize errors elsewhere. Reassuringly, error estimates are close to the actual differences in the withheld areas. Elsewhere, both analyses rely on much the same data, so the differences between them are likely to be smaller than the true analysis error.

Another check of internal consistency compares the difference between the solution and the data with the theoretical estimate of that difference given by formulae (17,16). In the points

where data were used in the OS analysis, the theoretical estimate is calculated according to (17). This estimate slightly exceeds the actual difference almost everywhere (not shown). The theoretical estimates inside withheld areas are computed according to (16), where the value of Π was estimated by (15) with cross terms neglected. In conclusion we find that the estimates in the withheld areas are in good agreement with actual values.

(b). Experiment with imitated data mask. In this experiment the OS was run for the period 1960–1991 with the data coverage information taken from the month exactly 60 years earlier. For example, in the analysis for July 1978 only observations in those areas which included data in July 1918 were used, and for those points observational error estimates were based on number of observations in 1918. The observed data were also contaminated by Gaussian noise, white in time and space, with the variance equal to the difference between the estimated observational error variances for the simulated and the actual time. Such an experiment is intended to check if results of the analysis during early periods, when data coverage was very poor, can be trusted. Results of the experiment are encouraging: whenever the OS has at least several data points in different parts of the analysis domain, it successfully recovers a complete structure, albeit with a slightly weakened amplitude. Figure 9 illustrates the results for January 1960 using data coverage information of January 1900. While the estimated anomaly amplitude has lowered and the error for a large part of the basin has doubled, the structure produced seems to be quite robust. Comparison between the OS and OI solutions (not shown) display some slight superiority of OS: the positive anomaly near the east coast of the US and the banded structure in the South Atlantic, however underdeveloped, are captured more correctly by the OS than by the OI in the test run.

If the data voids are extreme, as in July of 1978 (using the data coverage mask of 1918 – the end of the First World War and the apex of the influenza pandemic; Figure 10), OI cannot recover the structure in the southern part of the basin where there are no observations (not shown), but the OS field there is closer to reality. Note that even under these extreme conditions the analysis provides a realistic error estimate.

4.3 Application to the long record

We performed the OS analysis of the entire Atlantic SST anomaly record for 1856–1991, starting from the OI initial state. Figure 11 shows the result for selected months. The positive anomaly near Greenland in January 1856 is in an area where no data was available and so cannot be quite trusted (the OS error estimate in this area exceeds the magnitude of the anomaly). Analysis for 1885 looks trustworthy since the better part of the basin was already sampled at that time. The analysis for October 1918, has small amplitude and almost the same values as the error estimate. Such a result is not very useful, but is consistent with the observational data. The anomaly structure of February 1950 with amplitude of 1^o K is captured by analysis with a level of uncertainty generally under 0.2^oK.

Another application of this analysis is a reliable estimate of area averaged temperature. Figure 12 presents the monthly variation of the area average of the Atlantic SST north of 35^oN calculated from observational data and from the OS analysis. The latter is bounded by two curves corresponding to 99.7% confidence (3σ) intervals, where σ is estimated by the formula (18). Estimates obtained by straight averaging of available GOSTA data are inside the 99.7% limits when data coverage is sufficient (e.g. post 1950), but in the 19th century and the war years the averaging of available data is not an adequate estimate of the area average, and the analysis provides a more robust value.

5. Comparison of different methods

Four theoretical reduced space field estimates are defined in section 2.2 : $\mathcal{T}^p$, $\mathcal{T}^{\rm OI}$, $\mathcal{T}^a$, and $\mathcal{T}^s$. We compare them using as example, the SST field for February 1950. The first three of estimates are illustrated in the Figure 13; for the observed field and the OS solution $\mathcal{T}^s$ see Figure 11. When data are available for all gridboxes, all estimates are very close, because the accuracy of the MM is inferior to the data. The estimated analysis error steadily decreases as we progress from projection to OS.

The simplest of the estimates above, the projection estimate $\mathcal{T}^p$, is very similar to one obtained in Shriver and O'Brien (1995) and Smith et al. (1996). There are two important differences, however. First, the matrix $\mathcal{R}_n^{-1}$ is considered to be a simple weighting matrix

in those studies, while here it is derived from an extensive error analysis. In Shriver and O'Brien (1995) the matrix is diagonal with elements proportional to the *square* of the number of observations, while in Smith et al. (1996) it is an identity matrix. Omitting the statistical interpretation of the procedure means that their approach does not allow derivation of a theoretical error estimate $\mathcal{P}^p$.

A second difference is that in the cited studies the EOFs were calculated from a data set of higher quality than the one being analyzed: in Shriver and O'Brien (1995) EOFs from FSU analysis are used for COADS wind pseudostress analysis; in Smith et al. (1996) the analysis of COADS SST is based on EOFs from the NCEP OI analysis. In contrast, here we describe a method of reduced space analysis applied directly to the data set being analyzed, including the estimate of the data covariance matrix. This feature of our approach allows to derive EOF patterns from the longer samples than those usually associated with high quality data. Consequently, the results of the present analysis should be more robust and more suitable for studies of long-term climate variability.

Generally the Smith et al. (1996) SST analysis for 1950–1991 is close to our OS (Figure 14). Being constructed on the base of EOFs from the NCEP OI, it is approximately 0.05^oC closer to the NCEP OI solution than the reduced space OS in the spatial RMS, but in terms of spatial correlation both analyses are equally close to NCEP OI and are even closer to each other. When data coverage is good, all reduced space estimates give a similar answer.

If there are gaps in the data, or entire areas of the data are missing, the projection can create spurious anomalies in the areas of missing data because it tends to allow excessive variance in higher modes. As a result, it overfits existing data locally, and brings exaggerated variance to areas where the analysis is not restrained by observations. This is particularly true when a large number of EOFs are used. An example is February 1950 (Figure 13) where there is an area of missing data near 30^oS. Our analyses with 30 EOFs give larger magnitude of $\mathcal{T}^p$ in this area than $\mathcal{T}^{\rm OI}$, $\mathcal{T}^a$, and $\mathcal{T}^s$. A similar response was obtained by Smith et al. (1996) in their projection analysis for that month: a 1^oK negative anomaly appeared where data were missing. For areas of missing data, the projection method has no means for controlling spurious anomalies except by progressive reduction of the number of EOFs resulting in lower

resolution and diminished variance. The error estimate for the projection method (Figure 13) has a magnitude of 0.5^oC even for such a moderate sized area of missing data. This problem is discussed in Smith et al. (1996) as "overfitting," and "screening regression of varimax rotated EOFs" is suggested as a prospective solution. To some extent the problematic property of the projection method can be cured by putting zeroes in all data voids and setting the observational error equal to the field variance for all such quasi-observations. Results of such "improved projection" method are shown in Figure 13: the spurious anomaly of projection has disappeared and the level of the error in the area has decreased. The more complicated (OI, KF, and OS) methods of analysis provide regularization in a more systematic way, and their error estimates in the area are smaller.

Another way to monitor how the features of various scales are treated by different methods of analysis is to compare the energy in the calculated EOF amplitudes for different solutions with the estimates of that for the true signal (eigenvalues). These ratios are presented in Figure 15. While the projection method clearly generates excessive energy in small scales, the OI excessively damps it there (cf. Appendix B). The KF and OS are attempting to bring the ratios closer to unity, but do not make much change because the MM used damps high EOFs. However, since the high modes are responsible for only a small portion of the variance, the loss of total variance is not too large: is is about 6% for the OI solution and 5% for the OS.

The time dependence of theoretical error estimates (without the error of truncation) for different kinds of analyses (except for the projection method, which is an order of magnitude larger than other estimates) is shown in Figure 16: the top panel gives an average error over the basin, and the middle one shows the percentage of the area with error larger than 0.3^oK. The lower panel zooms in on the beginning of the period. Note that the KF computation started from the OI estimate, rather than the projection initial condition (10) in order to decrease the error in the very beginning of the run, and is equivalent to adding the "OI-like" term for the first month into the cost function.

The transfer to the reduced space improves time-continuity, since the leading spatial EOFs tend to capture slowly varying temporal modes, and some high-frequency noise gets filtered. Because of that $\mathcal{T}^{\mathrm{OI}}$ and even $\mathcal{T}^p$ are smoother in time than the observed data, being about as

smooth in time as the NCEP OI analysis is. However, the estimates $\mathcal{T}^a$ and $\mathcal{T}^s$ further improve the time-continuity of the solution.

6. Conclusion

The family of OI, KF, and OS, which all are popular methods of data analysis and are close relatives of the least squares method invented by Gauss, give optimal estimates in a very natural sense. These are usually considered as requiring both a great deal of (unavailable) information on the error covariance and unbearable computational expense in the case of application to large geophysical data sets. We have developed a systematic way to put a problem of estimating *projections* of a true field on a predetermined set of patterns (rather than a field itself) into the same classical context of a Gauss–Markov estimation scheme, and thus to obtain OI, KF, and OS solutions for these projections (which span a space of a reduced dimension). Since the set of patterns (we use the leading EOFs of the data) is chosen in a way that it is able to reproduce the large scale variability of the data on hand, we predominantly capture the features of those scales and filter out smaller scales as errors. While such solutions are formally suboptimal among full grid solutions, they are optimal among all reduced space solutions, being also far cheaper and much easier to feed a priori error covariance information. The tunable nature of the dimension of a reduced space allows keeping all scales down to the smallest resolved on the base of available data, and the choice of leading EOFs for a basis guarantees to some extent the minimal dimension of a space. Hence the savings of a reduced space analysis (compared to a full grid one) occur at the scales which are not really constrained by the data. Estimates on such scales are meaningless, but traditional schemes must compute them anyway.

Another advantage of a reduced space approach is that it facilitates modeling time transitions, if no model in a full grid representation is at hand.

On the basis of these theoretical considerations, we formulated a computationally efficient method for producing spatially and temporally coherent analyses of a historical data set. This method fills gaps in the data and minimizes sampling error. As a solution, it obtains a reduced space analogue for OS, and alternatively produces analogues for less complete estimates, i.e. the least squares fit to observations (projection), OI, and KF. In the described settings the method

can work successfully solely on the base of the data set to be analyzed, without use of additional higher-quality data. The drastic cost reduction as compared to the classical full grid OS made it possible analyze 136 years of the monthly Atlantic SST data (MOHSST5 – Bottomley et al. 1990, Parker et al. 1994) on a workstation. It is important to emphasize here the triple role which space reduction plays in our approach: it makes the OS procedure computationally feasible; it allows us to create a MM to incorporate time covariance information; and it acts as a data filter.

A strong advantage of the method, inherited from the classical least squares approach, is its ability to provide error estimates for analyzed data. In actual application to the Atlantic SST we made a series of tests which proved the method to be robust and consistent with its own error estimates. Verification against other analyses (available for relatively modern data only, e.g. Reynolds and Smith 1994, Smith et al. 1996) showed it to be similar to them in quality. However, there are reasons to believe that for early data the reduced space OS performs better than the other methods would.

The most important (and probably restrictive for some applications) assumption of the method in its described settings is a hypothesis that those patterns of space and time variability which are dominating in recent time (more precisely, in the time period used for computation of EOF patterns and creating the model for time transitions) were dominating in the early periods (which are poor in data coverage). The acceptability of such a hypothesis depends, of course, on the nature of the data, and should be considered separately for each application of the method.

Acknowledgments

This study has been supported by NOAA grants NA36GP0074, NA56GP0161, and UCSIO P.O. 10075411. We thank Michael Jackson and Robert Hackett of the U.K. Hadley Centre for making the MOHSST5 data available to us and for their assistance. Naomi Naik and Moshe Israeli provided generous help in issues of computational linear algebra algorithms. Keith Rodgers, Gilles Reverdin, and Dick Dee kindly read the manuscript and made many useful remarks and corrections. We thank three anonymous reviewers for valuable comments that helped improve the presentation of this paper. The help of Virginia DiBlasi-Morris and Moanna

St.Clair in preparing the manuscript is also appreciated.

Appendix A: The Optimal Smoother (OS) as a least squares estimate

If all estimated fields are put together into a huge single column vector $\tilde{\mathcal{T}} = [\mathcal{T}_1^T \mathcal{T}_2^T \dots \mathcal{T}_N^T]^T$, then all information contained in equations (1)–(2) can be rewritten as a single equation

$$\tilde{H}\tilde{\mathcal{T}} = \tilde{\mathcal{T}}^{o\,\mathrm{m}} + \tilde{\varepsilon}. \tag{A1}$$

To do so, we must reinterpret equations (2) as statements on "pseudo-observations" of model discrepancies; i.e. the vectors $(\mathcal{T}_{n+1} - A_n\mathcal{T}_n)$ are "observed" to be zero with "observational" errors $\varepsilon_n^{\mathrm{m}}$. Complete "observational" vector $\tilde{\mathcal{T}}^{o\,\mathrm{m}}$ concatenates vectors of real observations $\mathcal{T}_n^o$ and zero vectors corresponding to pseudo-observations of model discrepancies, while matrix $\tilde{H}$ provides transformation from a space of $\tilde{\mathcal{T}}$ to a space of vector $\tilde{\mathcal{T}}^{o\,\mathrm{m}}$, and thus consists of the blocks H_n, blocks $[-A_n\ I]$ (I is space×space identity matrix), and zero blocks.

By construction the error $\tilde{\varepsilon}$ will satisfy

$$\langle\tilde{\varepsilon}\rangle = 0, \qquad \langle\tilde{\varepsilon}\tilde{\varepsilon}^T\rangle = \tilde{R} \tag{A2}$$

where the covariance $\tilde{R}$ has a block-diagonal structure with blocks R_n and Q_n.

Equations (A1) and (A2) determine a Gauss–Markov scheme of generalized least squares estimation for $\tilde{\mathcal{T}}$ (see e.g. Mardia et al. (1979), Rao (1973)). The corresponding LSE is

$$\hat{\tilde{\mathcal{T}}} = \left(\tilde{H}^T\tilde{R}^{-1}\tilde{H}\right)^{-1}\tilde{H}^T\tilde{R}^{-1}\tilde{\mathcal{T}}^{o\,\mathrm{m}}, \tag{A3}$$

which minimizes the quadratic expression

$$\tilde{\mathbf{S}}[\tilde{\mathcal{T}}] = \left(\tilde{H}\tilde{\mathcal{T}} - \tilde{\mathcal{T}}^{o\,\mathrm{m}}\right)^T\tilde{R}^{-1}\left(\tilde{H}\tilde{\mathcal{T}} - \tilde{\mathcal{T}}^{o\,\mathrm{m}}\right).$$

The theoretical estimate of the error covariance for $\hat{\tilde{\mathcal{T}}}$ is

$$\tilde{P} = \left(\tilde{H}^T\tilde{R}^{-1}\tilde{H}\right)^{-1} \tag{A4}$$

Formulae (A3) and (A4) involve inversion of a block-tridiagonal matrix of large dimension. Solving linear systems with such matrices (finding $\hat{\tilde{\mathcal{T}}}$) can be achieved by a block version of the

"sweep" (Thomas) algorithm, which consists of two sequential runs across matrix rows of blocks in opposite directions. The Rauch–Tung–Striebel (RTS) algorithm for OS (Rauch et al. 1965) is basically a modification of the "sweep" method designed to produce both the field estimate $\hat{\tilde{\mathcal{T}}}$ and diagonal blocks of its error covariance matrix $\tilde{P}$.

Appendix B: Covariance of reduced space solutions

For those reduced space solutions which do not make use of the model for time transitions (the projection and optimal interpolation (OI)), it is easy to obtain explicit formulae for their covariance. These solutions have the form

$$\hat{\alpha} = \mathcal{P}\mathcal{H}^T\mathcal{R}^{-1}\mathcal{T}^o$$

(cf. (12) and (13)), where $\mathcal{P}$ is the theoretical estimate for the covariance of the error in $\hat{\alpha}$. Inserting (5) into this equation, we obtain

$$\hat{\alpha} = \mathcal{P}\mathcal{H}^T\mathcal{R}^{-1}\mathcal{H}\alpha + \mathcal{P}\mathcal{H}^T\mathcal{R}^{-1}\epsilon^o$$

where α is a vector of "true" projections of the field on EOF patterns, and thus its covariance is a diagonal matrix of eigenvalues Λ. Under assumptions formulated in section 2.2 and with the use of (13) and (7), the covariance of the estimate $\hat{\alpha}$ is

$$\langle\hat{\alpha}\hat{\alpha}^T\rangle = \mathcal{P}(\mathcal{P}^p)^{-1}\Lambda(\mathcal{P}^p)^{-1}\mathcal{P} + \mathcal{P}(\mathcal{P}^p)^{-1}\mathcal{P}$$

where, as before, $\mathcal{P}^p = (\mathcal{H}^T\mathcal{R}^{-1}\mathcal{H})^{-1}$.

Specific formulae for the projection and OI estimates (using (12) for the latter) are

$$\langle\alpha^p\alpha^{p\,T}\rangle = \Lambda + \mathcal{P}^p,$$
$$\langle\alpha^{\mathrm{OI}}\alpha^{\mathrm{OI}\,T}\rangle = \Lambda(\Lambda + \mathcal{P}^p)^{-1}\Lambda.$$

Interpretation of these results is straightforward: the covariance of the projection solution exceeds (in the sense of the footnote in section 2.2*(e)*) the "true" covariance Λ, while Λ exceeds the covariance of the OI. The same ordering is true for the variances of the EOF amplitudes, i.e. diagonal elements of covariance matrices (cf. Figure 15).

In the case of a one-dimensional reduced space the covariance matrix of projection error $\mathcal{P}^p$ becomes a scalar p^p, and we obtain

$$\langle (\alpha_1^p)^2 \rangle = \lambda_1 + p^p,$$
$$\langle \left(\alpha_1^{\mathrm{OI}}\right)^2 \rangle = \frac{\lambda_1^2}{\lambda_1 + p^p},$$

which gives a theoretical basis for tuning β in (19) by the requirement

$$\lambda_1 = \sqrt{\langle (\alpha_1^p)^2 \rangle \langle (\alpha_1^{\mathrm{OI}})^2 \rangle}.$$

Since the amplitude of the first EOF is a quite robust feature of the analysis, tuning can be inexpensively accomplished by performing the analyses with a one-dimensional reduced space and "old" (unchanged) eigenvalues λ'_m.

References

Barnett, T. P. (1984). Long-term trends in surface temperature over the oceans. *Mon. Weather Rev*, **112**, 303-312.

Blumenthal, M.B. (1991). Predictability of a coupled ocean-atmosphere model *J. Climate*, **4**, 766–784.

Blumenthal, M.B and M.A. Cane (1989). Accounting for parameter uncertainties in model verification: an illustration with tropical sea surface temperature. *J. Phys. Oceanography*, **19**, 815–830.

Bottomley, M., C.K. Folland, J. Hsiung, R.E. Newell, D.E. Parker (1990). *Global Ocean Surface Temperature Atlas*. HMSO, London

Cane, M.A., A. Kaplan, R.N. Miller, B. Tang, E.C. Hackert, and A.J. Busalacchi (1996). Mapping tropical Pacific sea level: data assimilation via a reduced state space Kalman filter. *J. Geophys. Res.*, **101**, 22599–22617.

Cheng, X., G. Nitsche, and J.M. Wallace (1995). Robustness of low-frequency circulation patterns derived from EOF and rotated EOF analyses. *J. Climate*, **8**, pp. 1709–1713.

Cohn, S.E., and R. Todling (1996). Approximate data assimilation schemes for stable and unstable dynamics. *J. Meteor. Soc. Japan*, **74**, pp. 63–75.

Dee, D.P. (1995). On-line estimation of error covariance parameters for atmospheric data assimilation. *Mon. Wea. Rev.*, **123**, 1128–1145.

Folland, C.K., D. E. Parker, F.E. Kates (1984). Worldwide marine temperature fluctuations 1865-1981. *Nature*, **310**, 670–673.

Folland, C.K. and D. E. Parker (1995). Correction of instrumental biases in historical sea surface temperature data. *Quart. J. Roy. Meteor. Soc.*, **121**, 319-367.

Fukumori, I., and P. Malanotte-Rizzoli (1995). An approximate Kalman filter for ocean data assimilation: An example with an idealized Gulf Stream model. *J. Geophys. Res*, **100**, 6777–6793.

Fukumori, I. (1995). Assimilation of TOPEX sea level measurements with a reduced-gravity, shallow water model of the Tropical Pacific ocean. *J. Geophys. Res*, **100**, 25027–25040.

Gandin, L.S. (1963). *Objective Analysis of Meteorological Fields.* Gidrometeorologicheskoye Izdatel'stvo, Leningrad. Translated from Russian, Israeli Program for Scientific Translations. Jerusalem, 1965. 242 pp.

Gelb, A. (ed.) (1974). *Applied Optimal Estimation.* MIT Press, Cambridge, MA. 374 pp.

Ghil, M., S.E. Cohn, J. Tavantzis, K. Bube, and E. Isaakson (1981). Applications of estimation theory to numerical weather prediction. In: *Dynamic meteorology: data assimilation methods.* Eds. L. Bengtsson, M. Ghil, E. Kallen. Springer–Verlag, New York, 139–224.

Householder, A.S. (1975) *The theory of matrices in numerical analysis.* Dover Publications, New York. 257 pp.

Jones, P.D., Wigley T.M.L., and Farmer, G. (1991). Marine and land temperature data sets: a comparison and a look at recent trends. In: *Greenhouse-gas-induced climatic change: a critical appraisal of simulations and observations.* Ed. M.E. Schlezinger. Elseiver, Amsterdam, 153–172.

Kalman, R.E. (1960). A New Approach to Linear Filtering and Prediction Problems, *Journal of Basic Engineering* (ASME), **82D**, pp. 35-45.

Laning J.H., Jr., and R.H. Battin (1956). *Random Processes in Automatic Control.* McGraw–Hill Company, Inc., New York, 269–275.

Legler, D.M. Errors in five-day mean surface wind and temperature conditions due to inadequate sampling (1991). *J. Atmos. and Ocean. Tech.*, **6**, 705–712.

Legler, D.M., I.M. Navon, J.J. O'Brien (1989). Objective analysis of pseudostress over the Indian Ocean using a direct-minimization approach. *Mon. Wea. Rev*, **117**, 709–720.

Lorenc, A. (1986). Analysis methods for numerical weather prediction. *Quart. J. Roy. Meteor. Soc.*, **112**, 1177–1194.

Mardia, K.V., J.T. Kent, and J.M. Bibby (1979). *Multivariate Analysis.* Academic Press, Inc., New York. 521 pp.

Miller, R.N. (1990). Tropical data assimilation experiments with simulated data: the impact of the tropical ocean and global atmosphere thermal array for the ocean. *J. Geophys. Res.*, **95**, 11,461–11,482.

North, G.R., T.L. Bell, R.F. Calahan, F.J. Moeng (1982). Sampling errors in the estimation of empirical orthogonal functions. *Mon. Wea. Rev.*, **110**, 699–706.

Parker, D.E., P.D. Jones, C.K. Folland, and A. Bevan (1994). Interdecadal changes of surface temperature since the late nineteenth century. *J. Geophys. Res.*, **99**, 14,373–14,399.

Preisendorfer, R.W. (1988) *Principal Component Analysis in Meteorology and Oceanography.* Elsevier, New York. 425 pp.

Rao, C.R. (1973) *Linear statistical inference and its applications.* John Wiley & Sons, Inc., New York. 625 pp.

Rauch, H.E., F. Tung, and C.T. Striebel (1965). Maximum likelihood estimates of linear dynamic systems. *AIAA J.*, **3**, 1445–1450.

Reynolds, R.W., and T.M. Smith (1994). Improved global sea surface temperature analysis using optimum interpolation. *J. Climate*,**7**, 929–948.

Sasaki, Y. (1970). Some basic formalism in numerical variational analysis. *Mon. Wea. Rev.*, **98**, 875–883.

Shapiro, R. (1971). The use of linear filtering as a parameterization of atmospheric diffusion. *J. Atmos. Sci.*, **28**, 523–531.

Shen S.S.P., G.R. North, K.-Y. Kim (1994). Spectral approach to optimal estimation of the global temperature. *J. Climate*, **7**, 1999–2002.

Shriver, J.F., J.J. O'Brien (1995). Low-frequency variability of the equatorial Pacific ocean using a new pseudostress dataset: 1930–1989. *J. Climate*, **8**, 2762–2786.

Smith, T. M., R. W. Reynolds, C.F. Ropelewski (1994). Optimal averaging of seasonal sea surface temperatures and associated confidence intervals (1860–1989). *J. Climate*, **7**, 949–964.

Smith, T. M., R. W. Reynolds, R. E. Livezey, and D.C. Stokes (1996). Reconstruction of historical sea surface temperatures using empirical orthogonal functions. *J. Climate*, **9**, 1403-1420.

Sorenson, H.W. (1970). Least-squares estimation: from Gauss to Kalman. *IEEE Spectrum*, **7**, pp. 63–68.

Talagrand, O. (1996). Assimilation of observations, an introduction. *J. Meteor. Soc. Japan*, submitted.

Thacker, W.C. and R. Lewandowicz (1996). Climatic indices, principal components, and the Gauss–Markov theorem. *J. Climate*, **9**, 1942–1958.

Trenberth, K.E., J.R. Christy, J.W. Hurrell (1992). Monitoring Global Monthly Mean Surface Temperatures. *J. Climate*, **5**, 1405–1423.

Wahba, G., D.R. Johnson, F. Gao, J. Gong (1995). Adaptive tuning of numerical weather prediction models: randomized GCV in three- and four-dimensional data assimilation. *Mon. Wea. Rev.*, **123**, 3358–3369.

Woodruff, S.D., R.J. Slutz, R.L. Jenne, and P.M. Steurer (1987). A comprehensive ocean–atmosphere data set. *Bull. Amer. Meteor. Soc.*, **68**, 521–527.

Xue Y., M.A. Cane, S.E. Zebiak, and M.B. Blumenthal (1994). On the prediction of ENSO: a study with a low-order Markov model. *Tellus*, **46A**, 512–528.

List of Figures

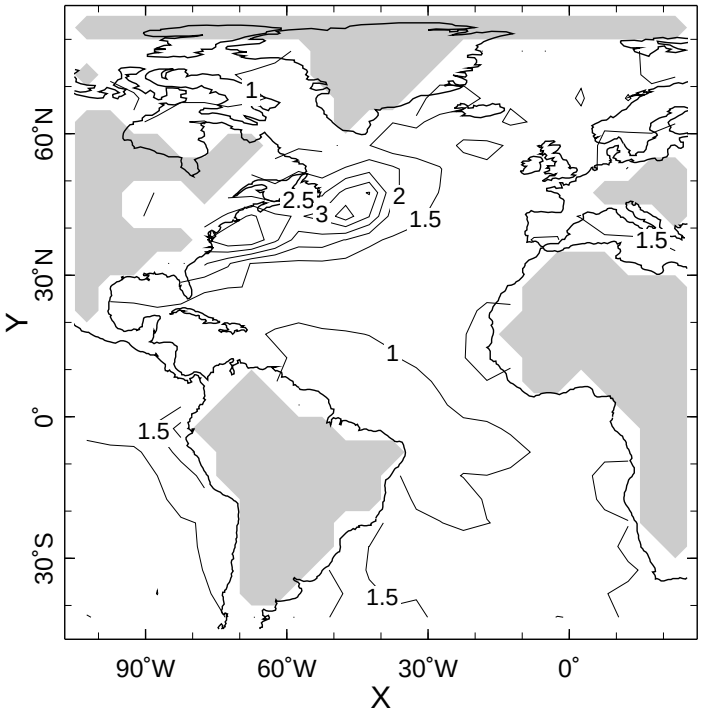

Figure 1. Intrabox variability estimates for monthly SST anomalies, ^{o}C

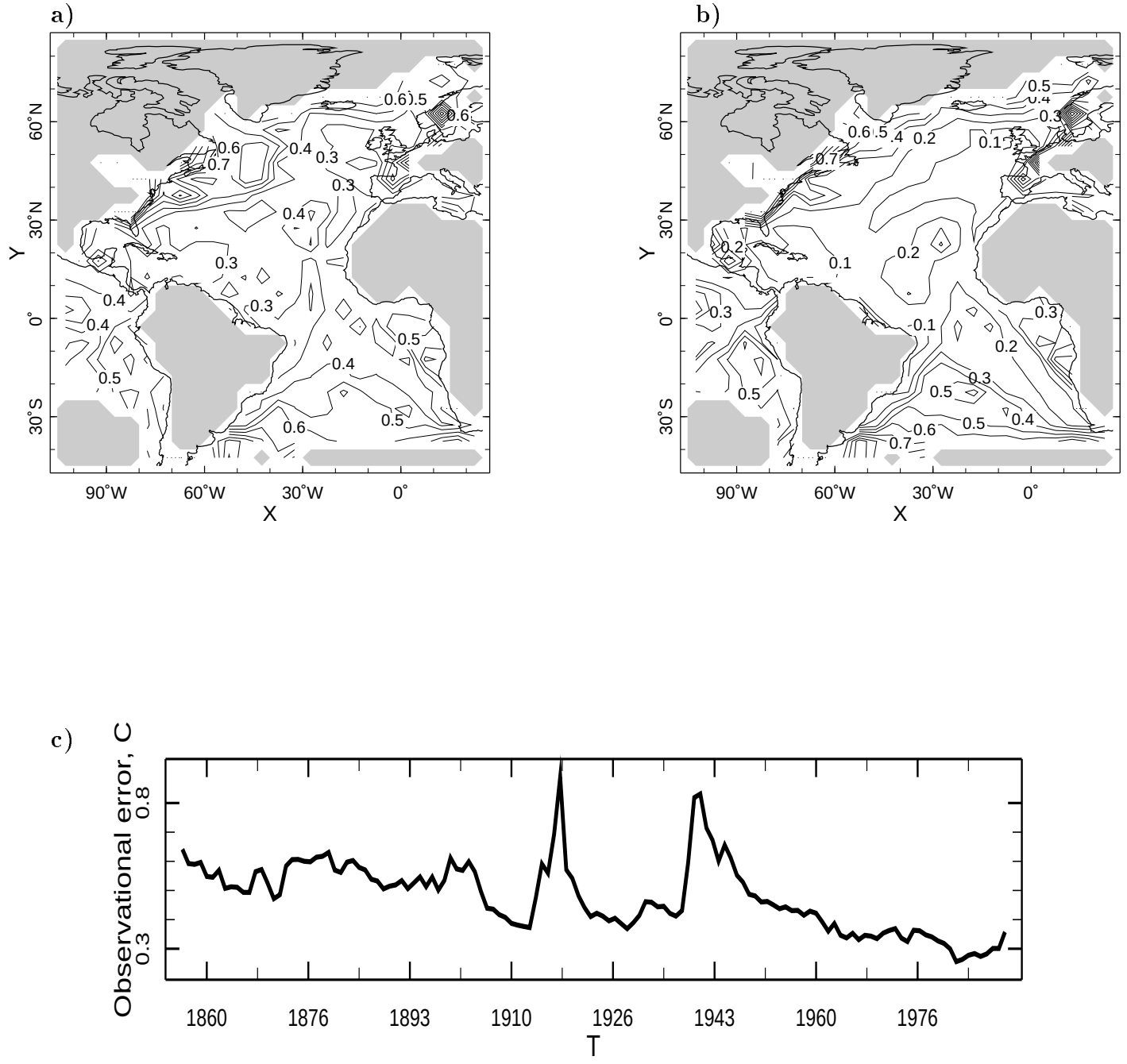

Figure 2. Rms of estimated data error, ^{o}C: *(a)* rms for 1856–1896, *(b)* rms for 1951–1991, *(c)* time dependence of spatial rms.

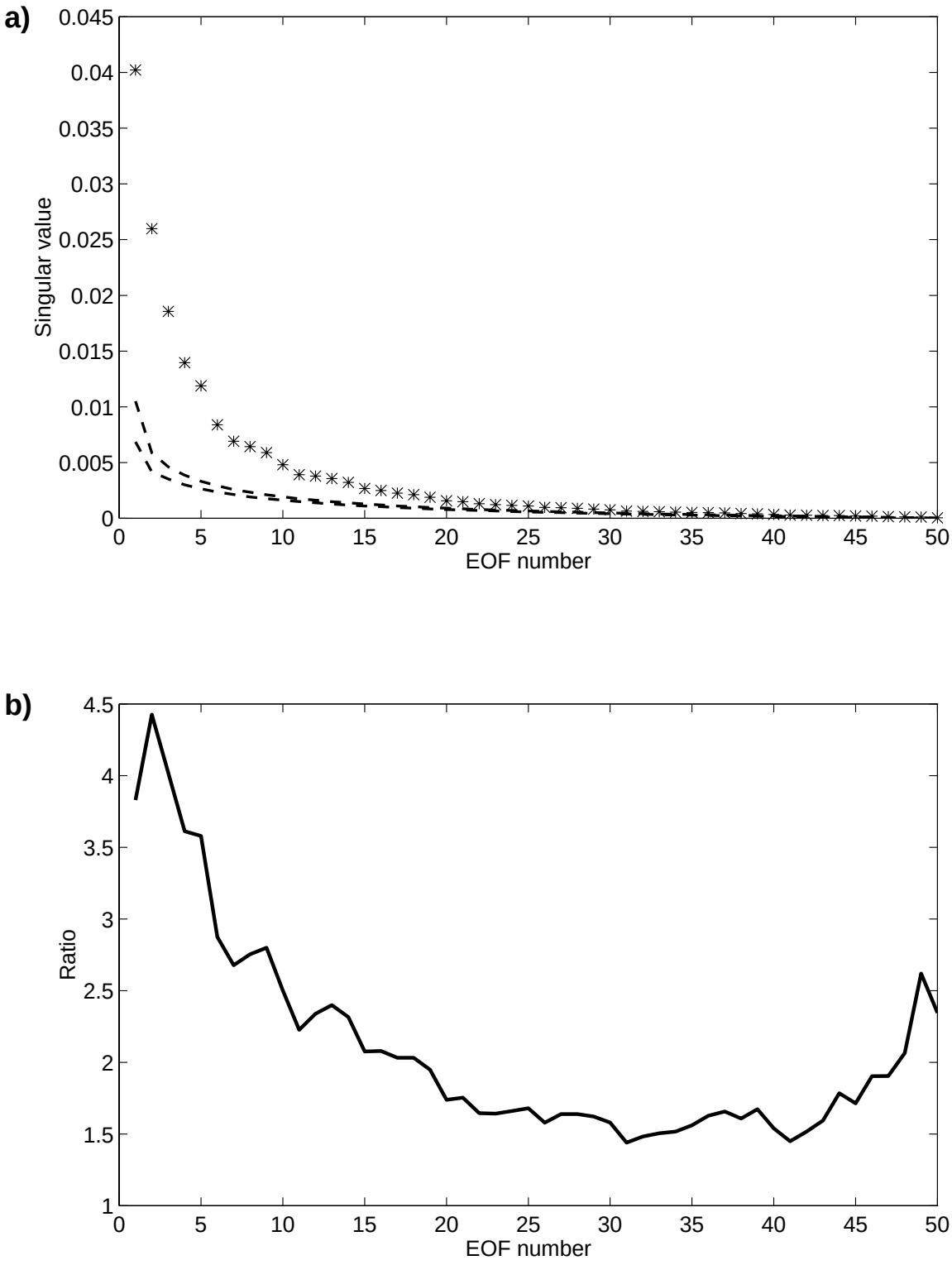

Figure 3. Significance check for singular values of the lag-one covariance matrix. *(a)* Singular values for the actual lag-one covariance matrix (asterisks) for the OI amplitudes as compared to those for reshuffled samples (dashed lines show the limits corresponding to top and bottom 5% of 500 random reshufflings). *(b)* The ratio of asterisks to the top dashed line from *(a)*.

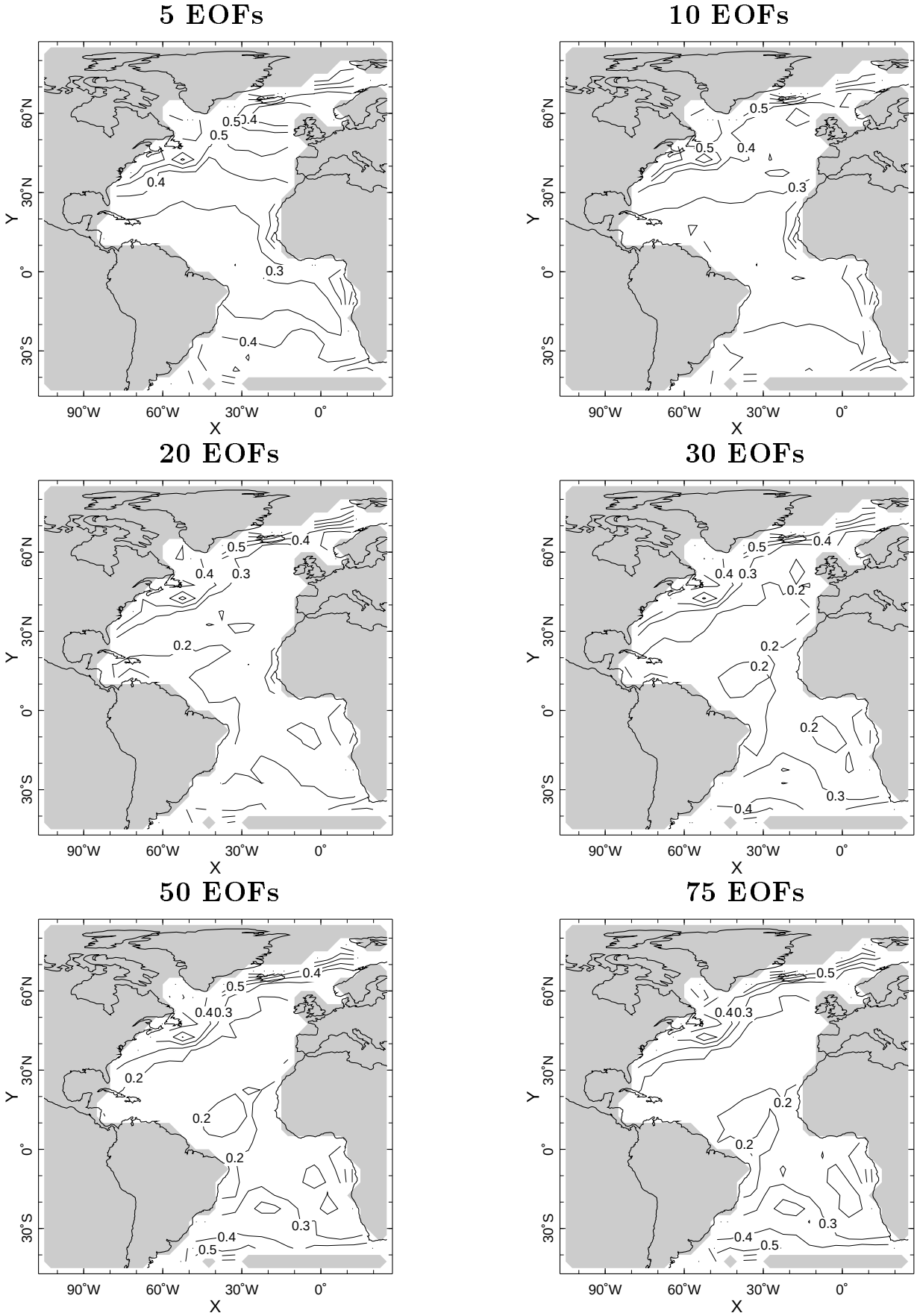

Figure 4. The rms differences between the NCEP OI solution and the reduced space OS analyses with 5, 10, 20, 30, 50 and 75 EOFs for the period 1982-1991

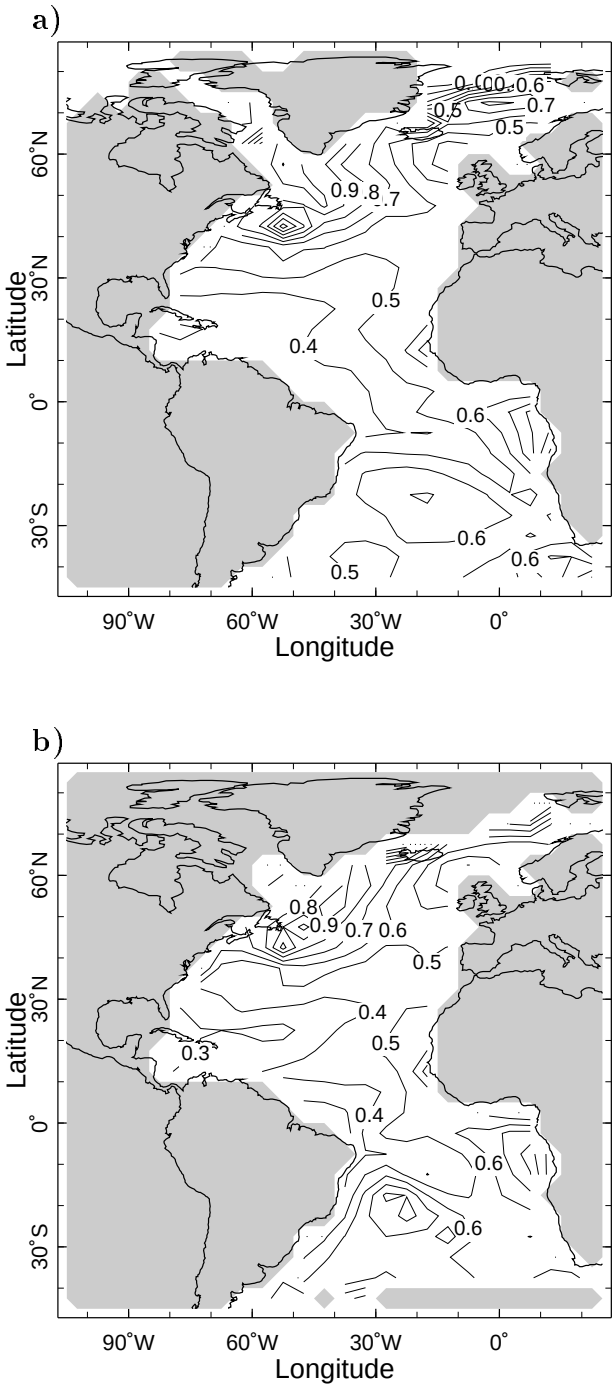

Figure 5. Rms SST resulting from *(a)* the NCEP OI and *(b)* present OS solution.

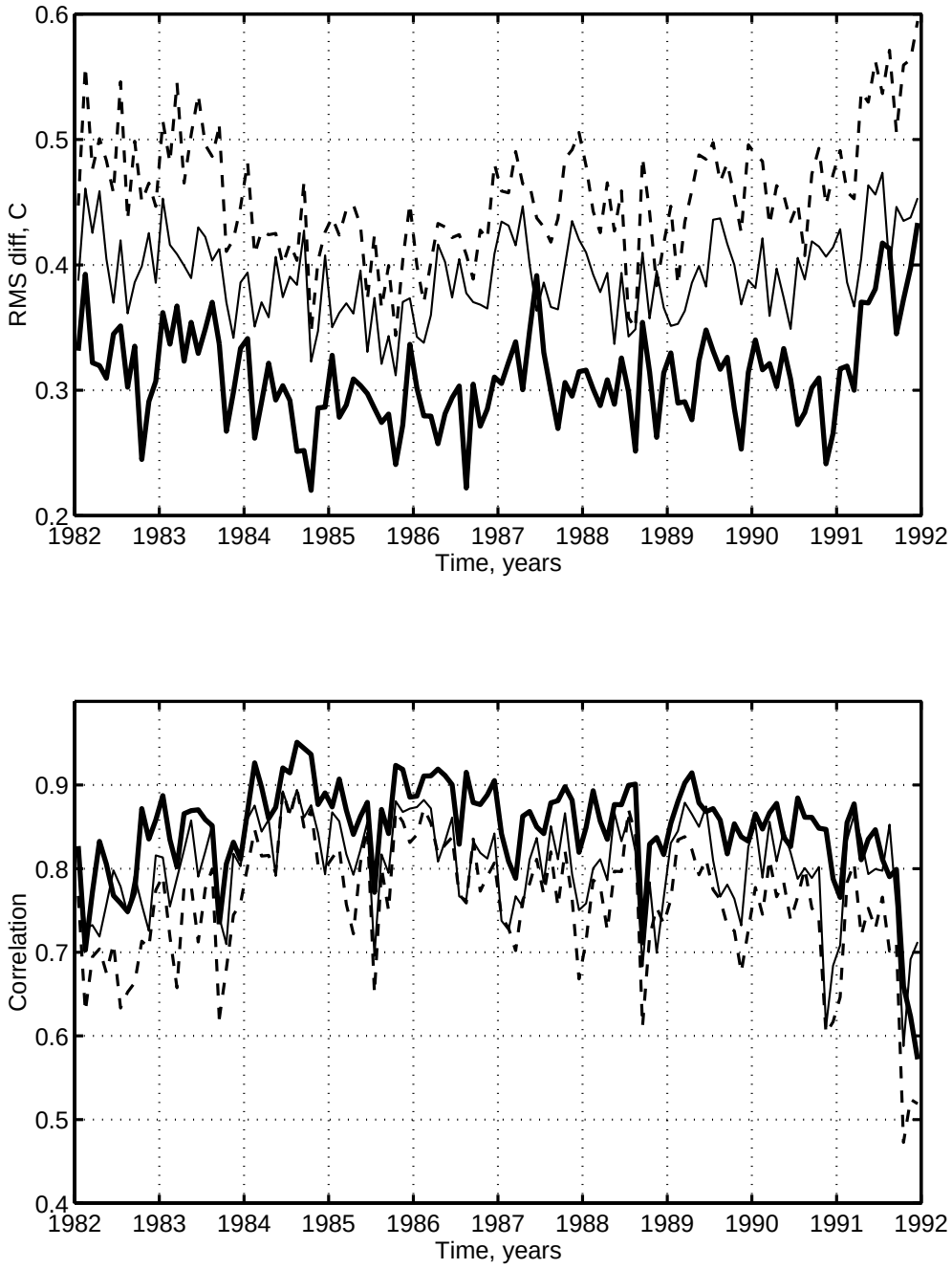

Figure 6. Rms difference and spatial correlation between the OS solution, NCEP OI analysis and raw GOSTA observations shown as a function of time from January 1982 to December 1991. The comparisons of the OS with the NCEP OI and observations are shown in thick and thin solid lines respectively. Dashed lines show the comparison between the NCEP OI and observations.

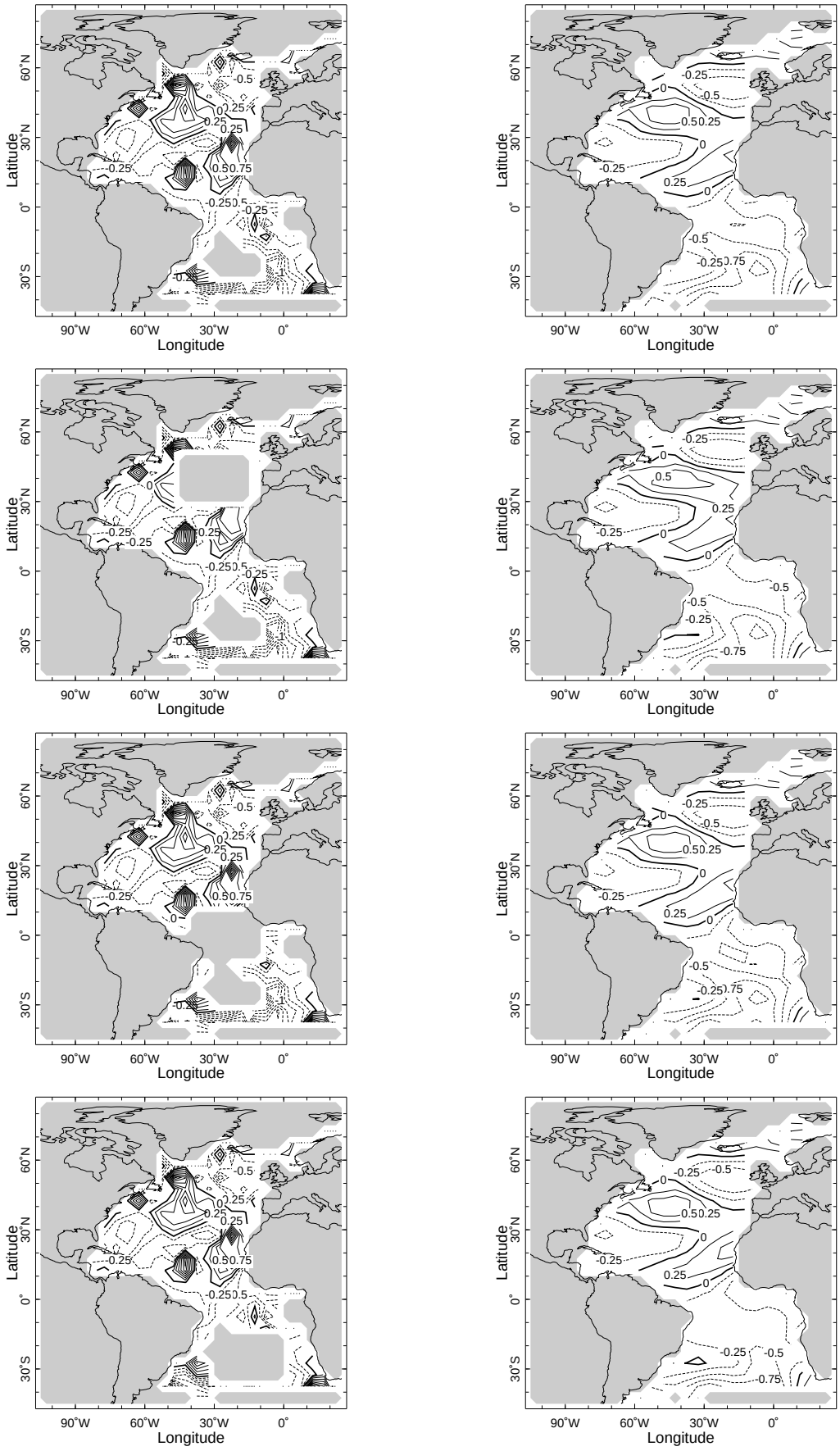

Figure 7. From top to bottom the October 1950 results of the OS analysis (right column) are shown for the observed SST field with full data and imposed northern, equatorial or southern $30^o \times 20^o$ degree artificial area of missing data (left column).

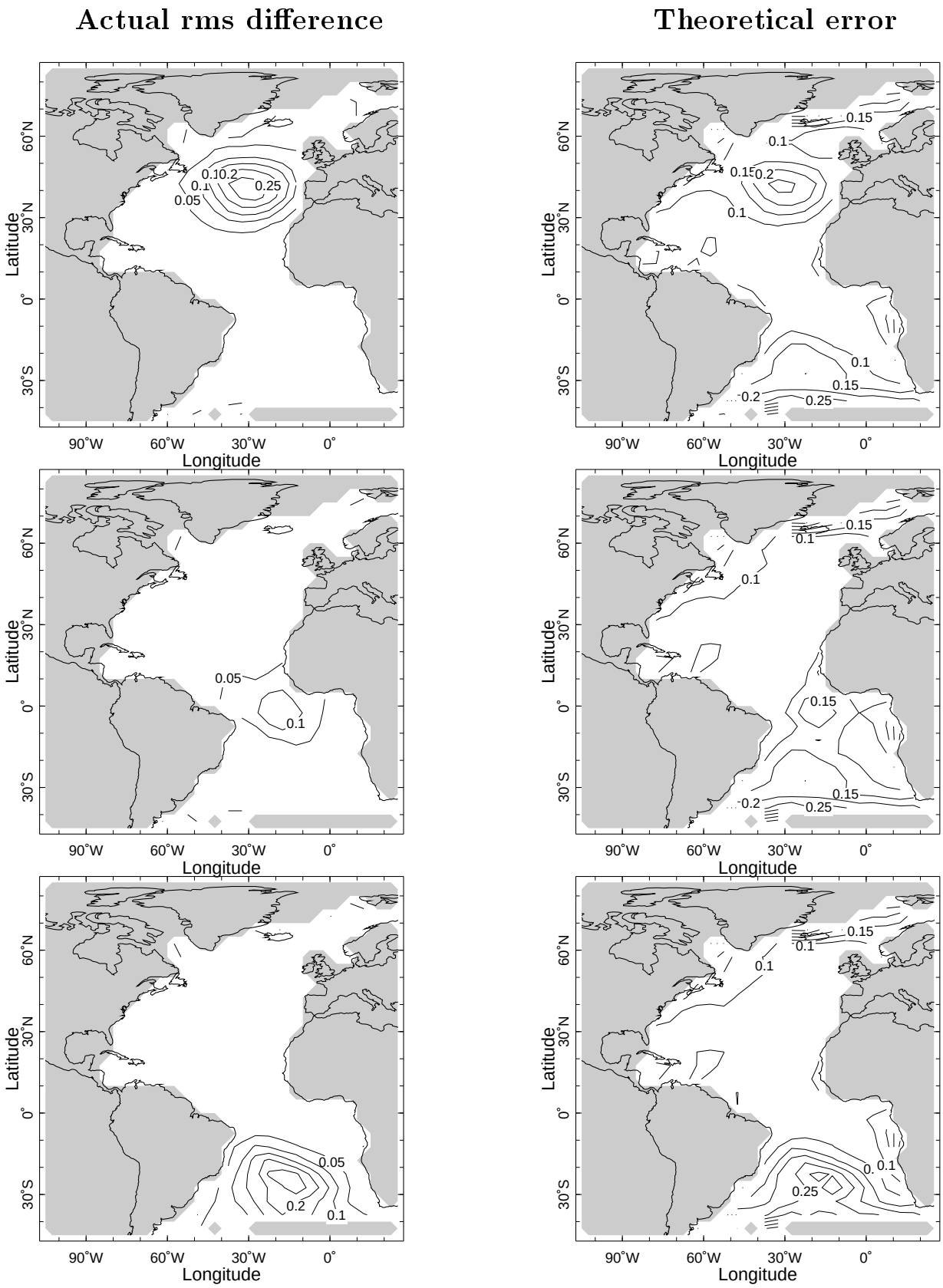

Figure 8. Rms differences for 1946–1991 between OS runs with and without withheld areas of Figure 7 (left column), and theoretical OS error estimates for runs with withheld areas (right column). Hereafter on all error maps we show only the error in scales corresponding to the 30 principal patterns which span the reduced space; full error would include the error of truncation (cf. (14) and (15))

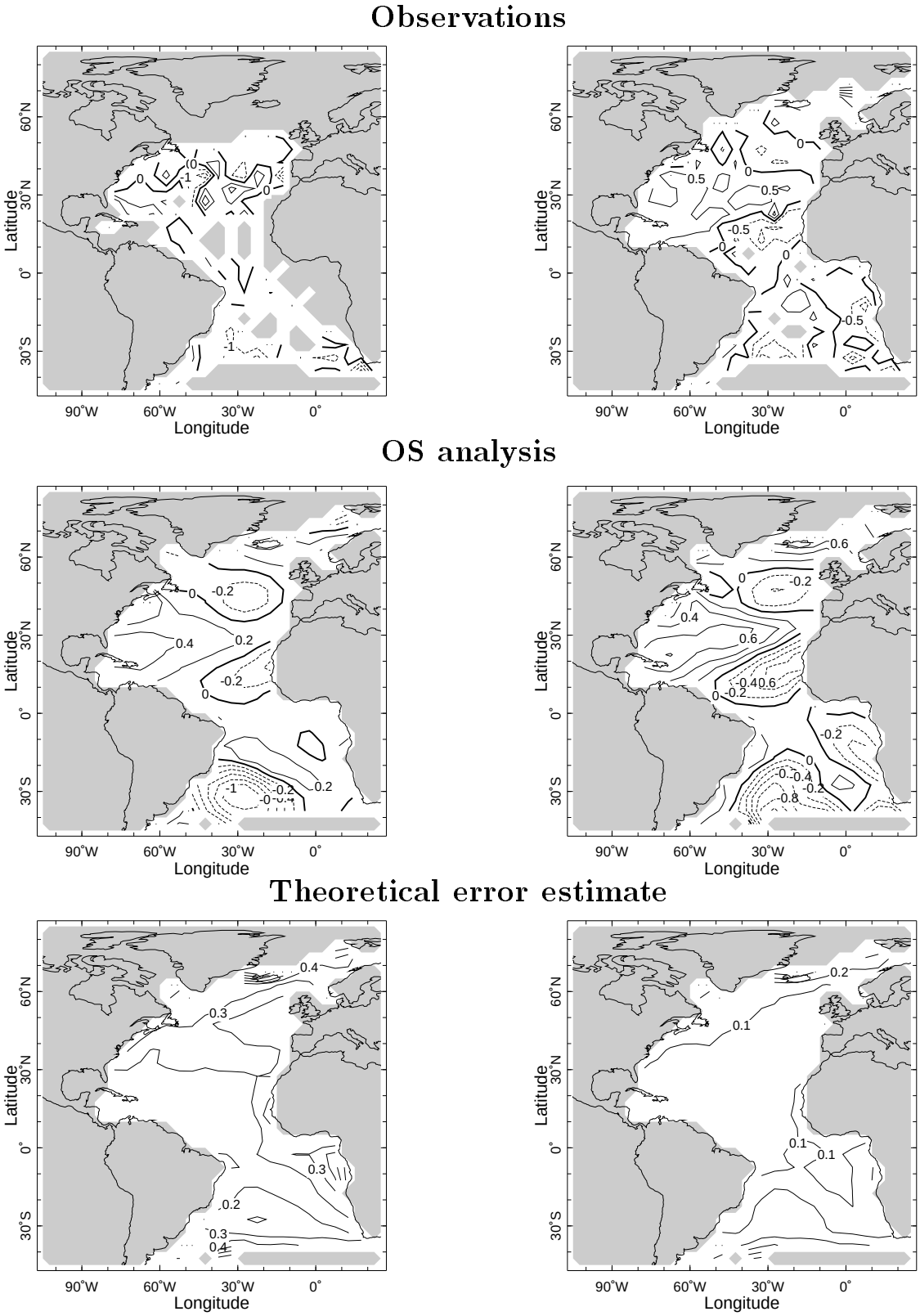

Figure 9. Results of the experimental run with recent data, but coverage mask taken from 60 years earlier (left panels) compared to the standard run (right panels). Shown are: observed data, OS solution and OS theoretical error estimate for January of 1960 (data mask of January 1900)

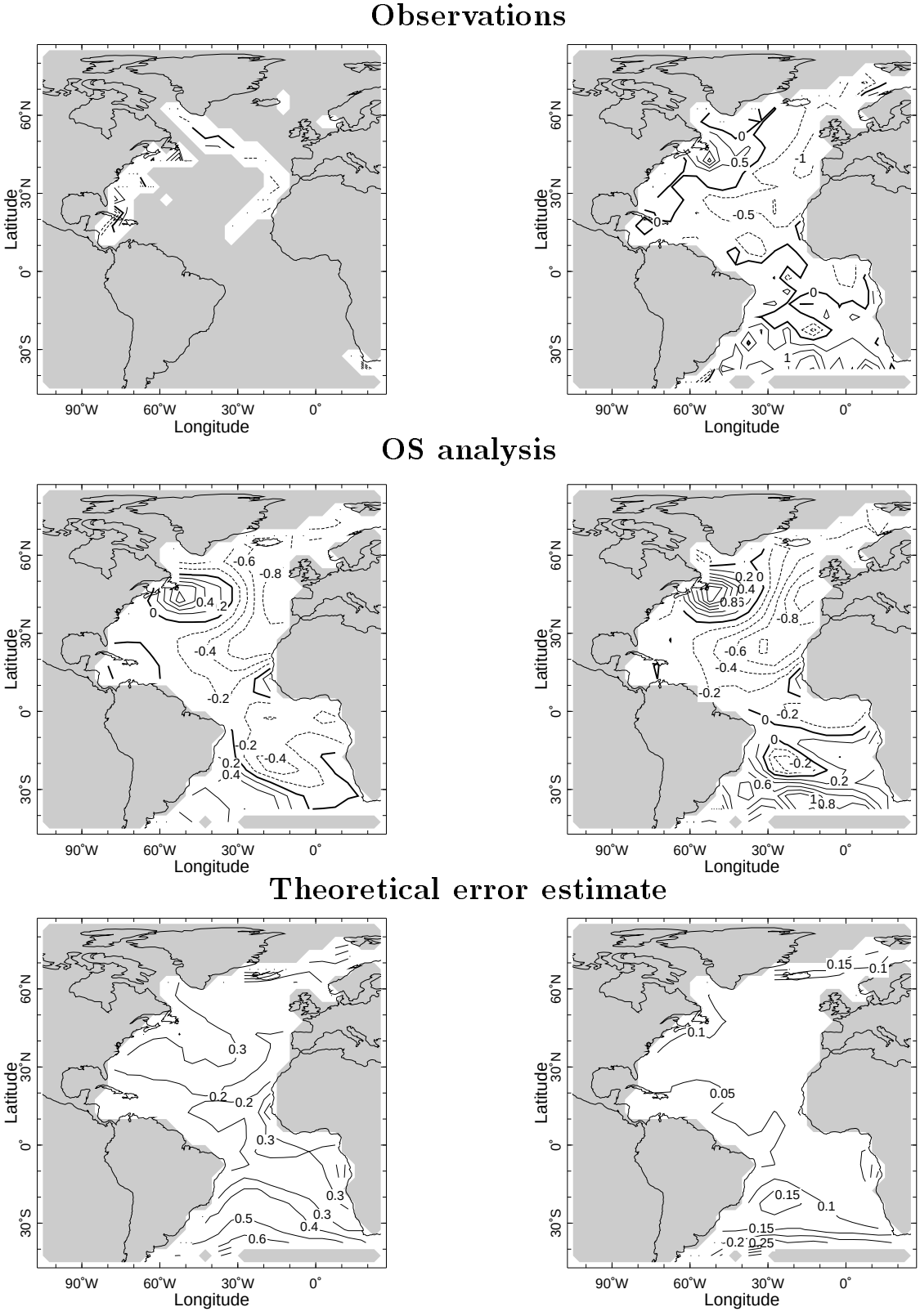

Figure 10. Same as Figure 9, but for July of 1978 (data mask of July 1918)

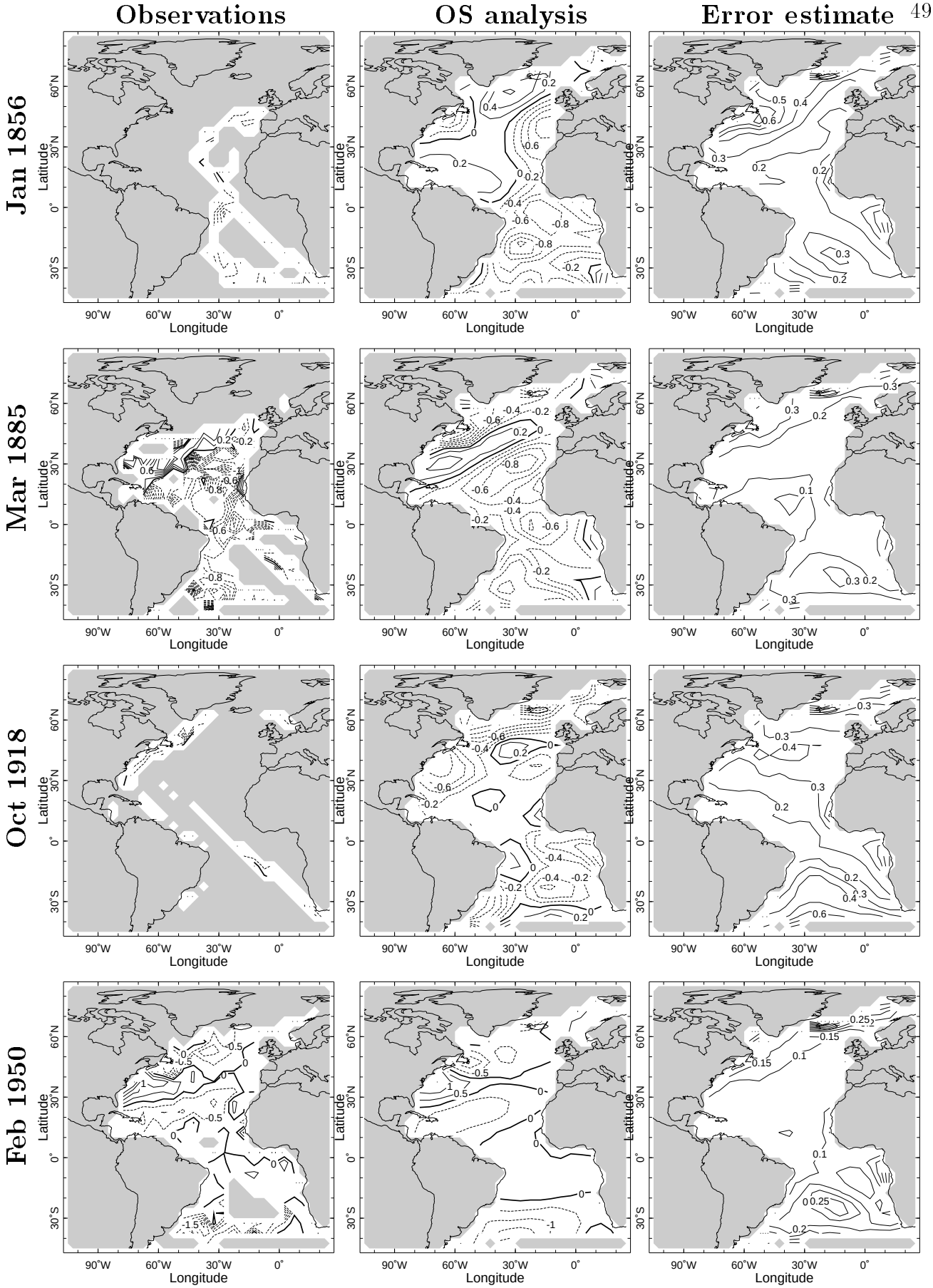

Figure 11. Results of the OS analysis applied to 136 years of the Atlantic SST record. Shown are an observed field, the OS analysis, and the OS error estimate for January 1856, March 1885, October 1918, and February 1950.

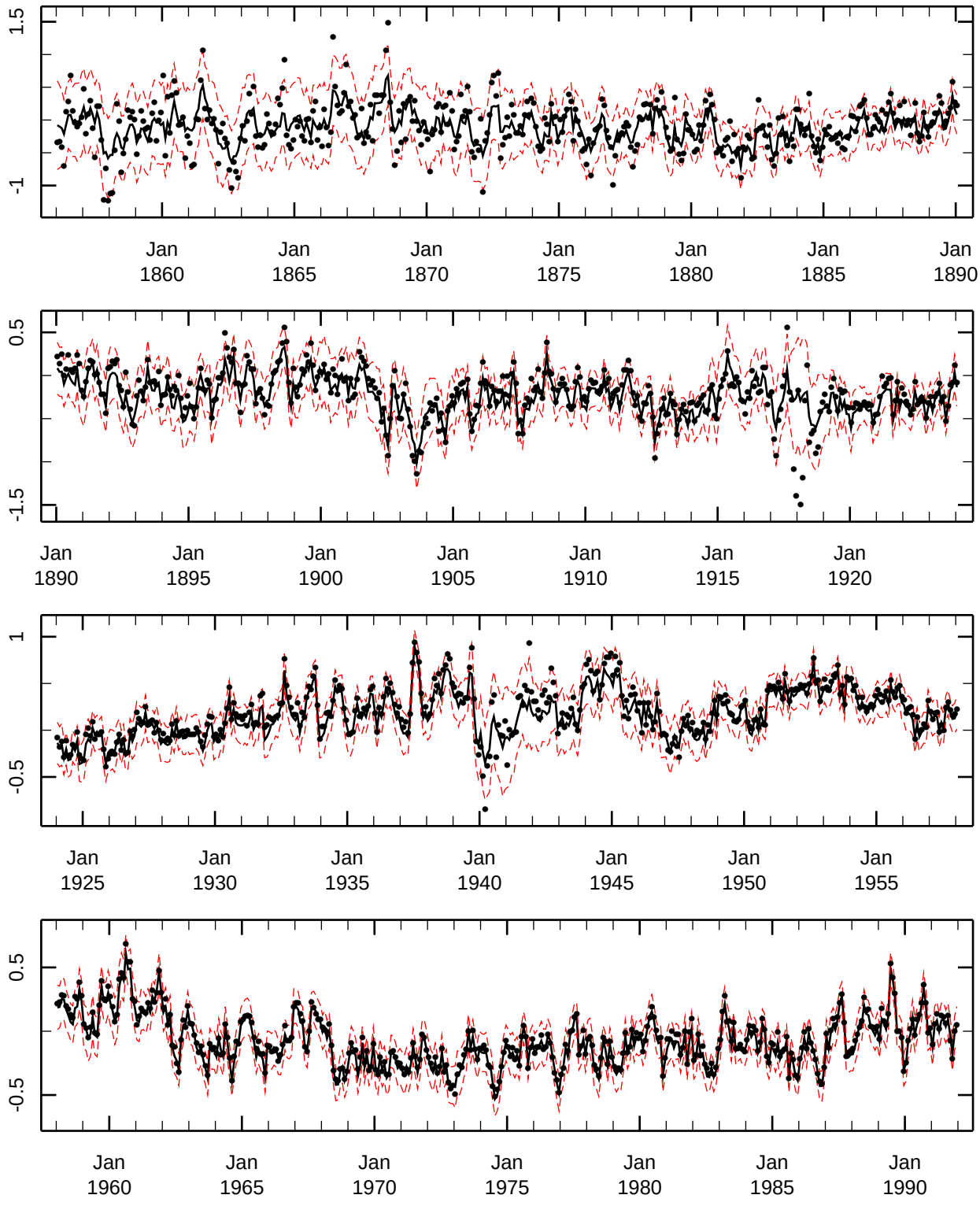

Figure 12. The North Atlantic area averaged SST anomaly (calculated to the north of 35N) for the MOHSST5 anomalies (bullets) and the OS estimate (solid line). 99.7% (3σ) confidence limits are shown by dashed lines.

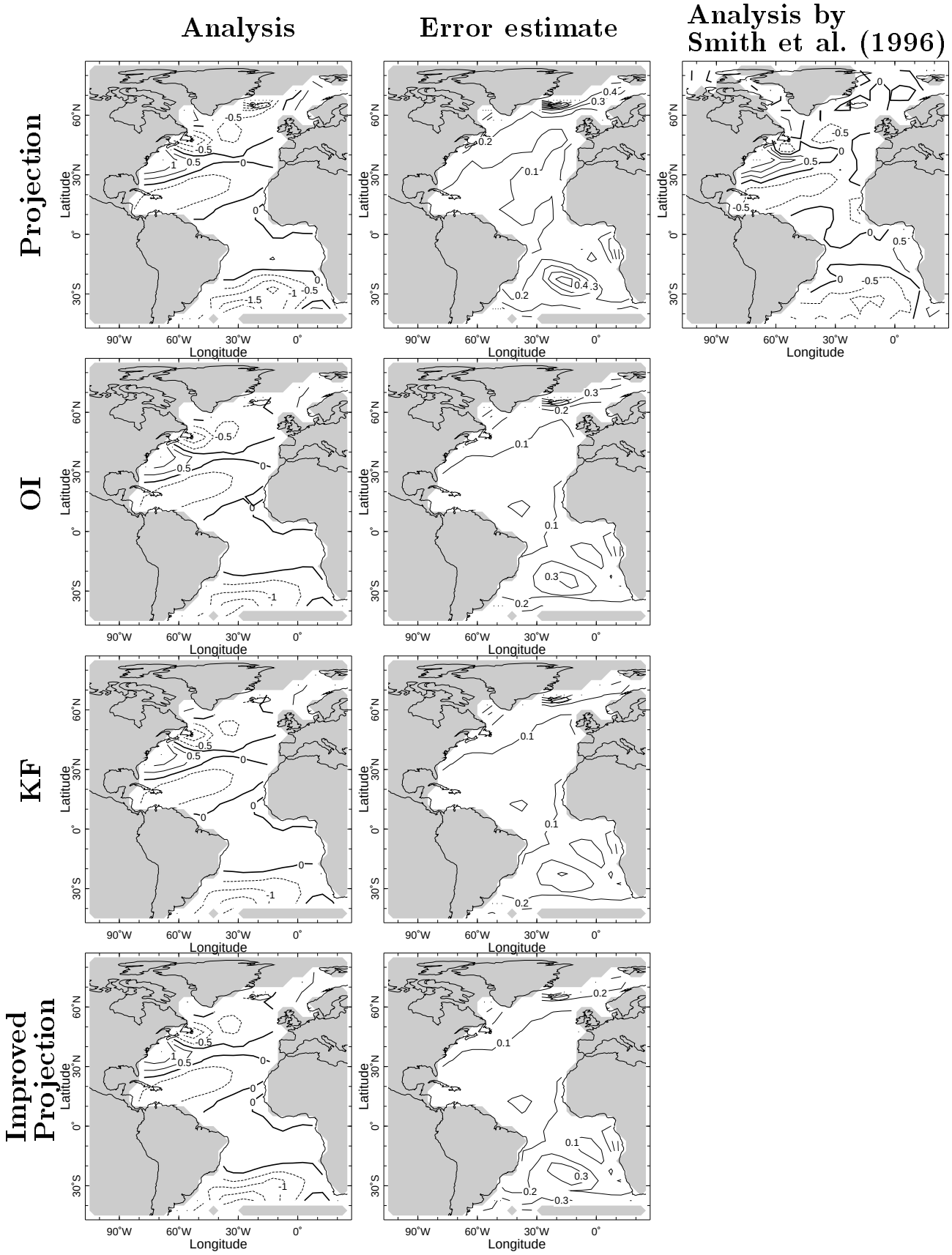

Figure 13. Various analyses results and error estimates for February 1950

a)

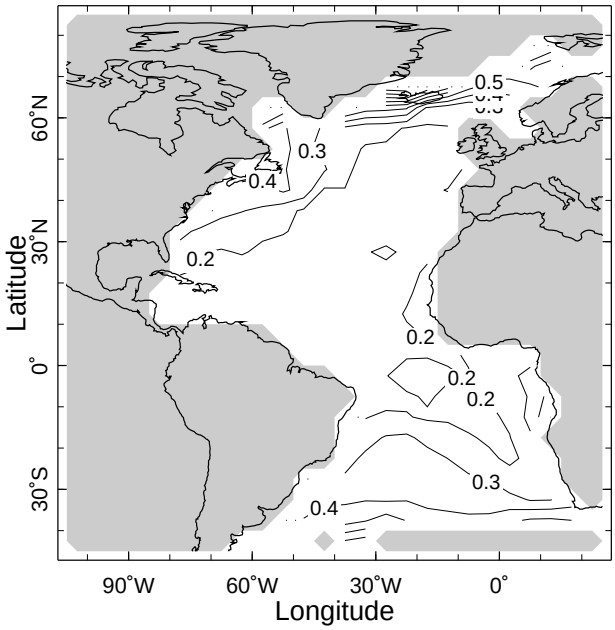

b)

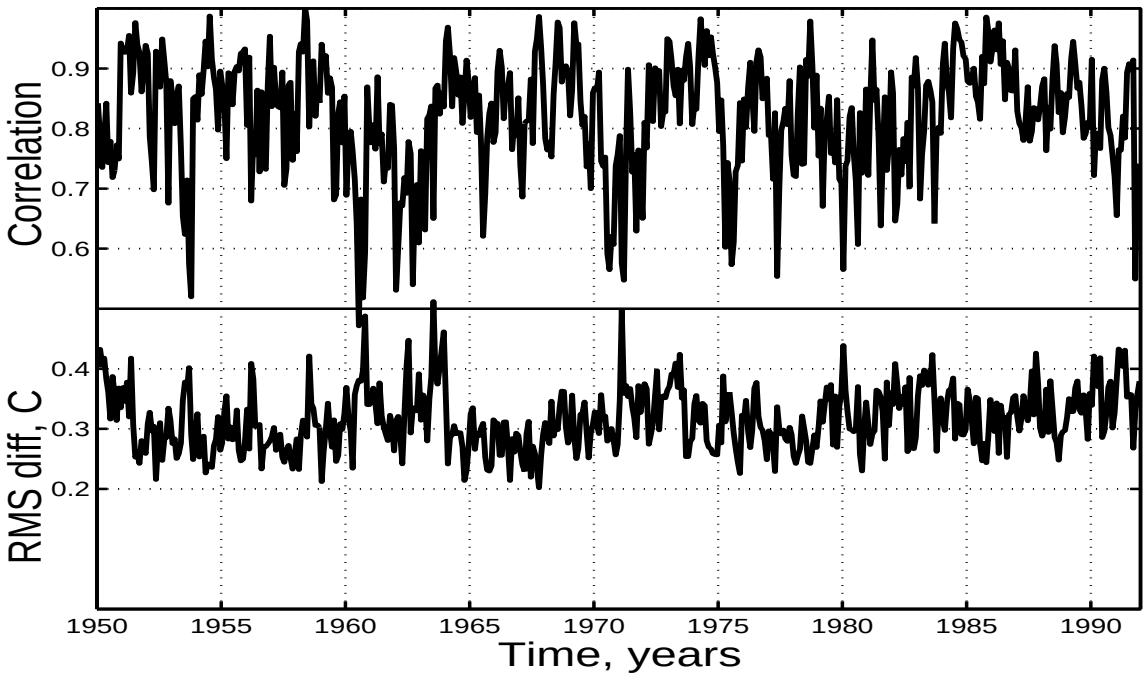

Figure 14. Comparison between Smith et al. (1996) and present OS analysis for the years 1950–1991: *(a)* the rms difference averaged over time; *(b)* Spatial rms and correlation as functions of time.

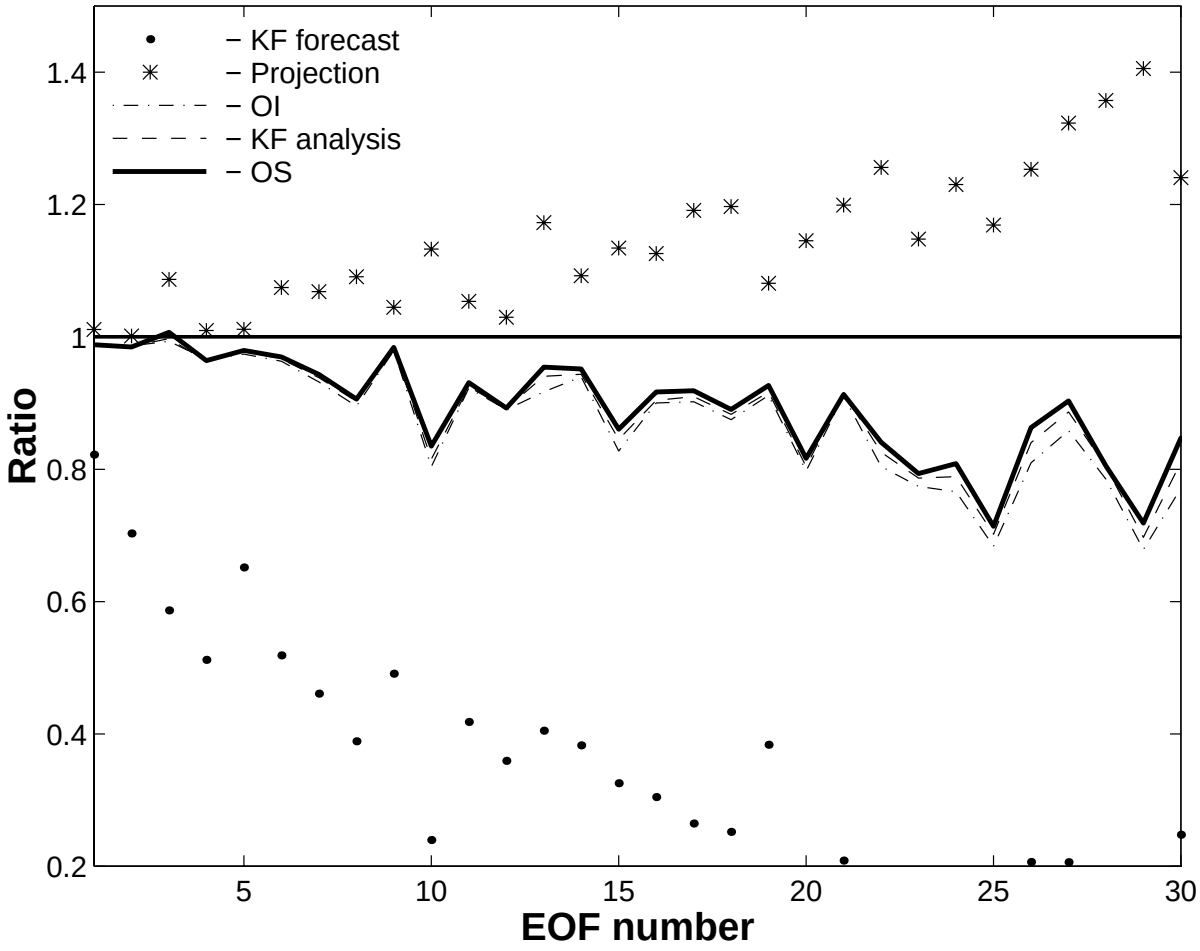

Figure 15. Energy in modes divided by eigenvalues of the estimate of the signal covariance matrix for various analyses

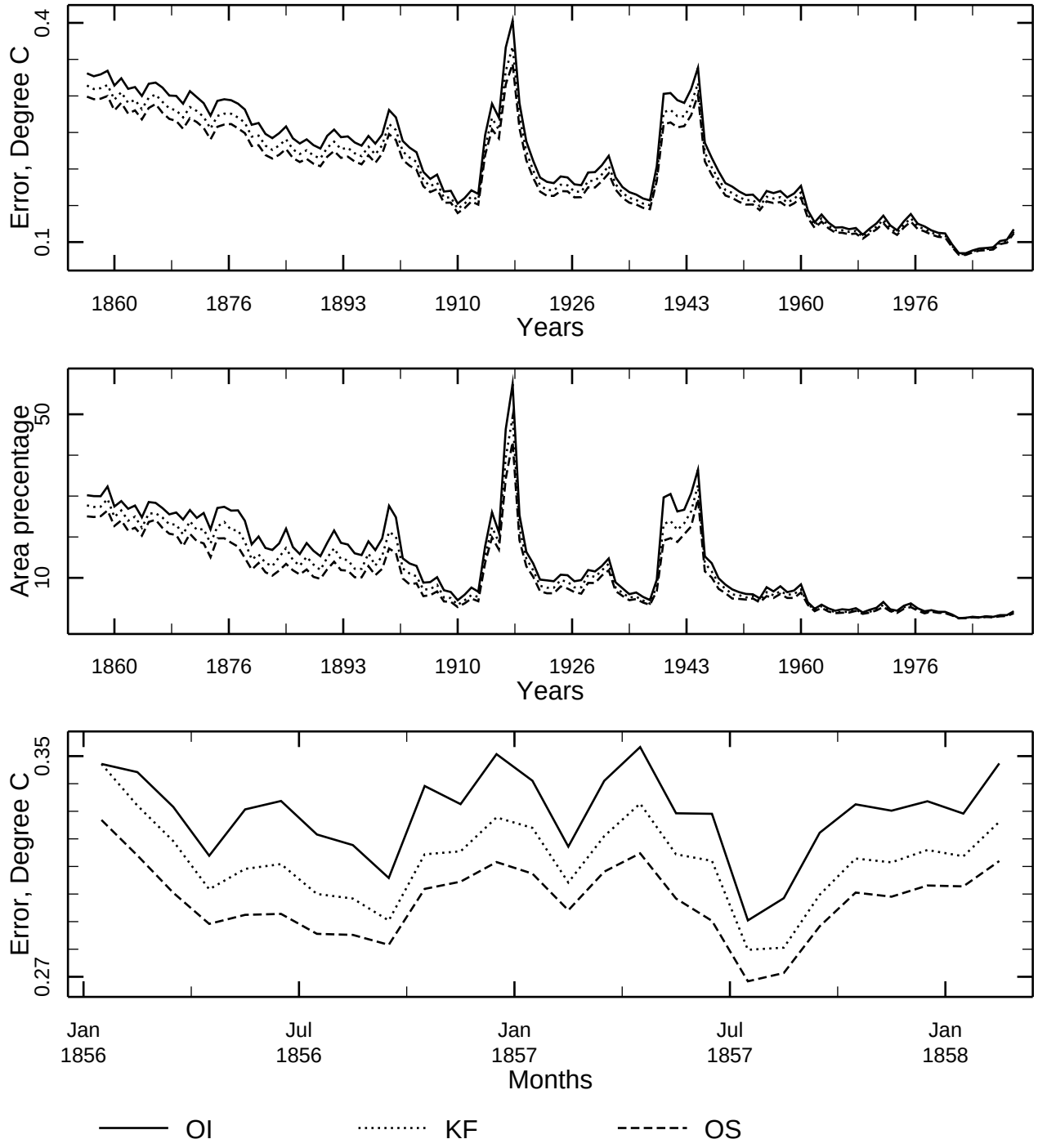

Figure 16. Theoretical error estimates for the reduced space OI, KF and OS analyses. Top panel – basin-averaged error estimates (annual means), middle panel – percentage of the area where the annual mean error exceeds 0.3^oK, lower panel – averaged error for the beginning of the period.